17

Soft Magnetic Materials

Soft magnetic materials are used extensively in power electronic circuits, as voltage and current transformers, saturable reactors, magnetic amplifiers, inductors, and chokes. These magnetic devices may be required to operate at only 50/60 Hz, or at frequencies down to dc or over 1 MHz. For example, a steel lamination ac mains voltage transformer operates at 50/60 Hz, while its ferrite switch-mode power supply equivalent may operate at 500 kHz. Soft magnetic materials have been utilised in other chapters for the following applications:

switching aid circuits	
- linear inductor	(8.3.3)
- saturable inductor	(8.3.4)
- snubber discharge	(figure 8.5)
- unified energy recovery	(9.2.1)
- thyristor *di/dt* control	(figure 8.5)
pulse transformers	(figures 7.7f)
current transformer	
turn-on snubber energy recovery	(figures 9.2a)
L-C resonator circuits	(figure 9.5c)
transient current sharing	(figure 10.8)
rfi filtering	(10.4.2)
single and three phase transformers	(11, 12)
cycloconverter intergroup reactors	(12.5)
phase shifting transformers	(14.1.3ii)
current source inductance	(14.2)
smps inductance and transformers	(15)

Hard magnetic materials, which are used for permanent magnets and ferrite beads for rfi suppression, are not specifically considered.

17.1 Material types

Two basic types of soft magnetic materials are extensively used, depending on the application and its requirements. These materials are:

- Ferromagnetic materials based on iron and nickel, which are for lower frequencies, < 2kHz, while
- Ferrimagnetic materials, which are based on ceramic oxides of metals, are applicable to frequencies from a few kilohertz to well over 80 MHz.

17.1.1 Ferromagnetic materials

17.1.1i - Steel

Cold-rolled grain-oriented steel is a 3-4 per cent silicon iron, cold reduced to develop a high degree of grain orientation, which gives

- increased flux for a given magnetising force and
- decreased size for a given rating, hence reduced weight.

Normally cores are produced in a number of material lamination thicknesses

- 0.3 mm for frequencies up to 200 Hz
- 0.1 mm for frequencies between 200 Hz to 2 kHz and
- 0.05 mm for higher frequencies and pulse applications.

Steel laminations for low frequency applications are available in different shapes. E and I laminations or strip C cores or toroids are extensively used for mains transformers and ac line inductors. Non-orientated silicon steels are extensively used for machine laminations.

17.1.1ii - Iron powders

Two general forms of iron powder cores are employed

- Cores are made by highly compacting insulated high quality spongy iron powder.
- High resistivity is required to reduce eddy current losses and so the iron powder is subjected to an acid treatment to produce an insulating oxide layer on the surface of each individual particle. This fine carbonyl iron is mixed with a bonding material and highly compressed. The bonding material used limits the maximum core temperature. Minute gaps appear between the particles, severely reducing the permeability. It is difficult to saturate such materials.

17.1.1iii - Alloy powders

These cores are made by highly compacting insulated alloy powder. The alloy is usually 50-75 per cent nickel, the remainder being iron with a small percentage of copper and molybdenum. The higher the iron percentage, the higher the saturation flux density and the higher the losses.

Powder iron and alloy cores are available in toroidal or ring shapes, cylindrical and hollow cylindrical cores, as well as cup cores, bobbins, pot cores, and beads.

17.1.2 Ferrimagnetic materials - soft ferrites

Ferrites are black, hard, brittle, chemically inert ceramic materials, which have a magnetic cubic structure.
The most general ferrites are polycrystalline magnetic ceramic oxides, which are compounds of iron oxide, Fe_20_3 mixed with one or more oxides of bivalent transition metals such as Fe0, Ni0, Zn0, Mn0, Cu0, Ba0, Co0, and Mg0. At lower frequencies, below a few MHz, a Mn-Zn combination is added to iron oxide, while for higher frequencies, above a MHz, Ni-Zn is the additive.
The raw oxide materials are mixed, pre-sintered at 1000°C if required, and ground. The powder material is shaped by means of pressing and sintering at between 1150°C and 1300°C. The sintering process involves raising the temperature to 1300°C in about 3 h, with 15 per cent oxygen present. The cores are cooled slowly without oxygen present to about 200°C in 20 h after entry. A 15 per cent linear, and 40 per cent by volume shrinkage occurs during sintering.
A diverse range of ferrite core shapes is available, which include, E, I, U, toroid, drum, pot, rod, tube, and screw. Where appropriate, diamond-wheel-ground air gaps are available on the centre pole. Manufacturing yields limit the physical component in size. Toroid cores of 152 mm outside diameter are not uncommon, and exotic shapes such as motor stators are made for special applications.

17.2 Comparison of material types

Table 17.1 shows typical comparative data for the main classes of soft ferro and ferri magnetic materials. Generally, those materials with higher saturating flux densities, B_s, have higher initial permeability μ_i, and hence offer higher inductance but at the expense of higher core eddy current and hysteresis losses.
Typical *B-H* curve characteristics are shown in figure 17.1 for the different soft magnetic materials shown in table 17.1. In the case of a transformer, the advantage of a high core flux density is that more volts v, per turn N, for a given frequency f, results. This is seen from Faraday's Law:

$$v = N\frac{d\phi}{dt} = NA\frac{d\,B}{dt} \qquad \text{(V)} \qquad (17.1)$$

whence for sinusoidal flux

$$v = 4.44NB_s A_c f \qquad \text{(V)} \qquad (17.2)$$

Table 17.1. Typical comparative data of soft magnetic materials

		Silicon steel	Iron		Alloys	Ferrites	
			powder	carbonyl		Mn-Zn	Ni-Zn
Frequency range, Δf	Hz	20-1k	400-10k	50k-1M	40-70k	400-250k	200k-10M
Temperature range, ΔT	°C	-55 to 300	-55 to 125	-55 to 105	-55 to 200	-30 to 105	-55 to 250
Initial permeability, μ_i		500	90	35	160	2700	100
flux density, B_s @ 25°C	T	1.75	0.86	0.86	0.63	0.47	0.24
remanence, B_r	T	1.2	0.2	0.001	0.02	0.2	0.12
Intrinsic mmf strength $H_i = (B_s - B_r)/2\mu_i$	A/m	440	2560	9120	1448	40	350
Resistivity, ρ	Ωcm	0.1				100	10^5 - 10^6
Curie temperature, T_c	°C	300	200	150	500	200	450

Inductance is specified from equation (17.1) and from

$$v = L\frac{di}{dt} \qquad \text{(V)} \qquad (17.3)$$

$$L = N\frac{d\phi}{di} \qquad \text{(H)} \qquad (17.4)$$

Using $\phi = BA_e$ and $H\ell_e = Ni$, equation (17.4) becomes

$$L = \frac{N^2 A_e}{\ell_e} dB\Big/dH \qquad \text{(H)} \qquad (17.5)$$

where dB/dH is the slope of the *B-H* curve, according to $B = \mu_o\mu_i H$. Therefore, before core saturation

$$L = \frac{N^2 A_e}{\ell_e}\mu_o\mu_i \qquad \text{(H)} \qquad (17.6)$$

The subscript ***e*** is used to denote the effective core parameter, as shown in table 17.2.
In rfi suppression and filtering applications, silicon steel is not effective since the initial permeability, μ_i, falls rapidly with frequency hence at the high suppression frequency, inductance is small. Thus iron powder or a high iron alloy may be used, which have relatively high flux densities and high losses. For rfi suppression, a high core loss aids suppression.
At inaudible frequencies, >20 kHz, for a low core loss, ferrites are extensively used. Although ferrite flux densities are relatively low, typically 0.4 T, eddy current and hysteresis losses are low. The low eddy current loss results from the high core material resistivity. With ferromagnetic materials, the eddy current loss is reduced by using thinner laminations or electrically isolated powder particles. A major disadvantage of a ferrite core is its poor temperature stability and low allowable core temperature. On the other hand, high initial permeabilities, >12,000, are obtainable.

Ferrite materials, application, and component design are specifically considered, although the concepts developed are generally applicable to ferromagnetic materials.

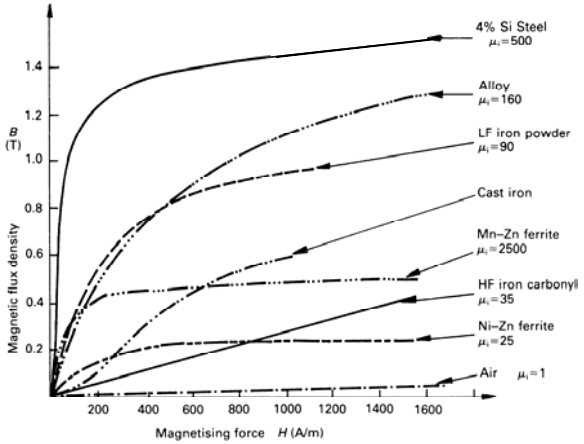

Figure 17.1. *Magnetisation curves for soft magnetic materials.*

17.3 Ferrite characteristics

The definitions and explanations given are applicable to soft magnetic materials in general and are illustrated specifically by reference to ferrite materials.
General mechanical and thermal properties of ferrites are given in appendix 17.6.

17.3.1 Dimensions and parameters

The effective magnetic dimensions are constant for a given core and are defined in table 17.2. These effective constants are based on the length ℓ and area A of the individual limbs comprising the complete core. These effective dimensions are used for magnetic component design, such as transformer core loss, which is given per unit effective volume, V_e.

Table 17.2. Core effective dimensions and parameters

core factor			
ℓ_e/A_e	c_1	$\Sigma\ell/A$	m^{-1}
effective area	A_e	$c_1/\Sigma\ell/A^2$	m^2
effective length	l_e	$A_e c_1$	m
effective volume	V_e	$\ell_e A_e$	m^3
core permeance	c	μ_o/c_1	H

From the parameters in table 17.2, inductance is calculated from equation (17.6) as

$$L = \mu_i c N^2 \quad \text{(H)} \tag{17.7}$$

17.3.2 Permeability

Figure 17.1 shows that a non-linear relationship exists between B and H for magnetic materials, and is characterised by the dimensionless parameter μ_r - the relative permeability - according to $B = \mu_o \mu_r H$ (where $\mu_o = 4\pi\times10^{-7}$ H/m). Figure 17.2 shows a detailed B-H magnetising curve for a ferrite material along with its hysteresis loop. The case of an air core magnetic circuit, for which $\mu_r = 1$, is also shown.
Figure 17.2 illustrates various definitions for μ_r based on

$$\mu_r = \frac{1}{\mu_o}\frac{B}{H} \tag{17.8}$$

17.3.2i - Initial permeability, μ_i

The initial permeability, which is dependant on temperature and frequency, is the permeability at weak field strengths at $H = 0$ and ΔH tends to zero, that is

$$\mu_i = \left[\frac{1}{\mu_o}\frac{\Delta B}{\Delta H}\right]_{H=0,\,\Delta H\to 0} \tag{17.9}$$

17.3.2ii - Amplitude permeability, μ_a and maximum permeability, $\hat{\mu}$

The amplitude permeability applies to large magnitude sinusoids, with no dc field applied, and is the ratio of the sinusoid peak B and H

$$\mu_a = \left[\frac{1}{\mu_o}\frac{\hat{B}}{\hat{H}}\right]_{H=0} \tag{17.10}$$

$\hat{\mu}$ is the maximum μ_a obtainable for any H, that is, $\hat{\mu}$ = max [μ_a] for all values of H. The variation of amplitude permeability with magnetising force or flux density is shown in figure 17.3. Because of the non-linear nature of the B-H curve loop, the amplitude permeability is highly dependant of the applied field strength magnitude.

This figure 17.3 is representative of a ferrite material suitable for a wide range of power electronic applications. More technical data for this material is presented in Appendix 17.7 and in the figures that follow.

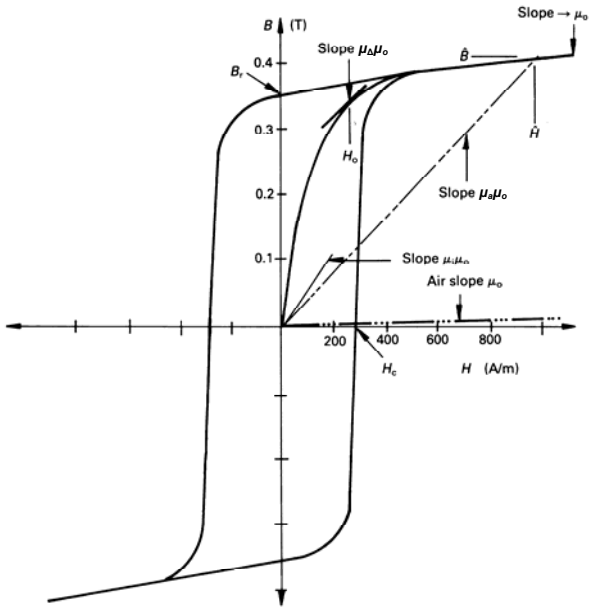

Figure 17.2. *Hysteresis loop illustrating permeability definitions, remanence B_r, and coercive force H_c.*

17.3.2iii - Reversible or incremental permeability, μ_{rev}, μ_Δ

When a core is magnetised with a polarising dc offset field upon which a small ac field is superimposed, the ac *H* field produces a small lancet-shape hysteresis loop which reduces to a straight line as the ac *H* field is reduced. The slope of this line, shown in figure 17.2, is called the incremental or reversible permeability

$$\mu_\Delta = \frac{1}{\mu_o} \lim_{\Delta H \to 0} \left[\frac{\Delta B}{\Delta H} \right]_{H\ =\ \text{constant}} \qquad (17.11)$$

The incremental permeability, μ_Δ is a function of the dc magnetic bias, as shown in figure 17.4. It is usually a maximum when no dc field is present, while for a toroid it is identical with the initial permeability, μ_i. With increased current, μ_Δ, hence inductance, decreases.

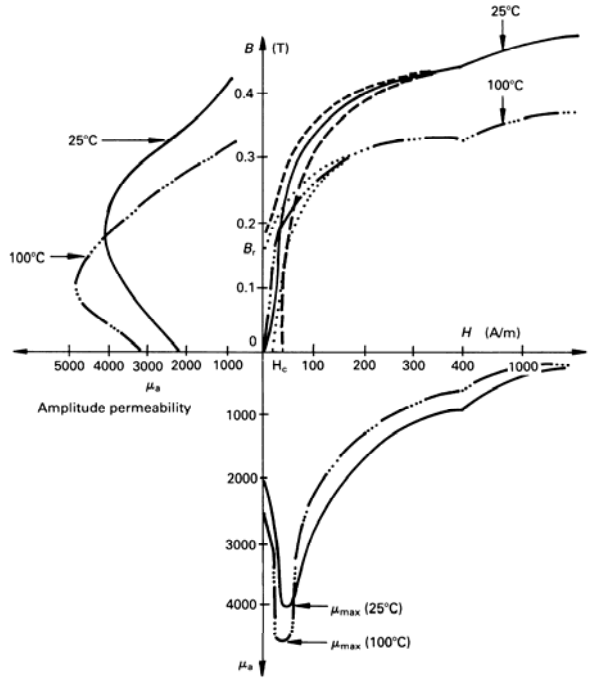

Figure 17.3. *Temperature dependence of flux density and permeability, μ_a.*

17.3.2iv - Effective permeability, μ_e

The inductance of a coil with a gapped core of effective permeability μ_e is given by

$$L = \frac{\mu_o \mu_e N^2}{\sum \ell / A} = \mu_e c N^2 = \mu_e L_o = A_L N^2 \qquad \text{(H)} \tag{17.12}$$

hence

$$\mu_e = L / cN^2 = L / L_o \tag{17.13}$$

where L_o is the coil inductance if the core is removed, whence the permeability drops. The term A_L is the inductance factor and is equal to $\mu_e c$. Conversely

$$N = \alpha \sqrt{L} \tag{17.14}$$

where $\alpha = 1/\sqrt{A_L}$ and is termed the turns factor.

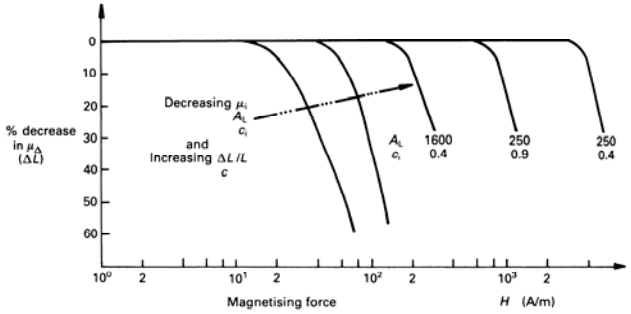

Figure 17.4. *Variation of permeability with field strength.*

If the air gap, ε, is small compared with the core of length, l_e, such that $\varepsilon << \ell_e$, the effective permeability approximates to

$$\frac{1}{\mu_e} = \frac{1}{\mu} + \frac{\varepsilon}{l_e} \tag{17.15}$$

The introduction of an air gap is equivalent to connecting two inductors in parallel: one without an air gap, μL_o; the other also without a gap but having an inductance $(l_e/\varepsilon)\, L_o$. The effective permeability of a gapped core at low flux levels is specified by the initial permeability, μ_i, and is given by

$$\frac{1}{\mu_e} = \frac{1}{\mu_i} + \frac{\varepsilon}{l_e} \tag{17.16}$$

The effective permeability for high flux densities is expressed in terms of the amplitude permeability, μ_a, that is

$$\frac{1}{\mu_e} = \frac{1}{\mu_a} + \frac{\varepsilon}{l_e} \tag{17.17}$$

That is

$$\mu_e = \frac{\mu_a}{1 + \frac{\varepsilon\, \mu_a}{\ell_e}} \tag{17.18}$$

A fringing factor, ε/β, must be introduced for significant gap widths, to account for the effective increase in permeability due to the fringing flux effect.

17.3.2v - Complex permeability, $\overline{\mu}$

Because of core losses, a coil can be represented by

- a series L_s - R_s circuit for an inductor
- a parallel R_p // L_p circuit for a transformer.

Core losses are modelled by the inclusion of resistance and the associated losses can be accounted for by considering the coil permeability as a complex variable, $\overline{\mu}$. For the inductor series equivalent circuit

$$Z = R_s + j\omega L_s = j\omega \overline{\mu} c N^2 \qquad (\Omega) \tag{17.19}$$

such that

$$\begin{aligned} \overline{\mu} &= \mu_s' - j\mu_s'' \\ &= \frac{L_s}{cN^2} - j\frac{R_s}{\omega c N^2} \end{aligned} \tag{17.20}$$

while for the transformer parallel equivalent circuit

$$\frac{1}{Z} = \frac{1}{R_p} + \frac{1}{j\omega L_p} \qquad \text{(S)} \tag{17.21}$$

such that

$$\begin{aligned} \frac{1}{\overline{\mu}} &= \frac{1}{\mu_p'} - \frac{1}{j\mu_p''} \\ &= \frac{1}{L_p / cN^2} - \frac{1}{jR_p / \omega c N^2} \end{aligned} \tag{17.22}$$

Since the parallel and series circuits are equivalent

$$\frac{\mu_s''}{\mu_s'} = \frac{\mu_p'}{\mu_p''} = \tan\delta \tag{17.23}$$

where tan δ is the core loss factor

$$\tan\delta = \frac{R_s}{\omega L_s} = \frac{\omega L_p}{R_p} = \frac{1}{Q} \qquad (17.24)$$

The complex permeability components are related according to

$$\mu_p' = \mu_s' \left(1 + \tan^2\delta\right)$$
$$\mu_p'' = \mu_s'' \left(1 + 1/\tan^2\delta\right) \qquad (17.25)$$

For low losses, namely at low frequencies, $\tan^2\delta \rightarrow 0$ in equation (17.25), whence $\mu_p' = \mu_s'$, while at high losses, at high frequencies, $\mu_p'' = \mu_s''$ since $\tan^2\delta \rightarrow \infty$ in equation (17.25). Complex permeability characteristics are shown in figure 17.5. The cut-off frequency, f_c is defined as the frequency at which the permeability is half the initial permeability, μ_s', at low frequency. At 25°C, f_c for Mn-Zn materials is approximated by $f_c \approx 4000/\mu_i$ (MHz), for μ_i at low frequency.
The complex permeability components are measured at low flux densities. Mn-Zn ferrites applicable to power application usually have high permeability, low resistivity, and a high dielectric constant. In such cases, the complex permeability is highly dependent on the core dimensions, as shown in figure 17.5, which characterises stacked toroids. Because of the associated large volume, volume resonance occurs where eddy currents dominate losses.

17.3.3 Coercive force and remanence

The coercive force H_c is the field strength at which the hysteresis loop cuts the H-axis as shown in figures 17.2 and 17.3. It is representative of the static hysteresis loss of the material. The point where the hysteresis loop intersects the B-axis is called the remanence, B_r. Where a core is operated with a magnetic field strength bias, for example, as with an inductor carrying dc current, the value of flux density is reduced to B_s - B_r for calculations. The area within the hysteresis loop represents core hysteresis loss, in Joules per unit volume.

17.3.4 Core losses

17.3.4i - Core losses at low H

At low magnetising forces, the total losses, represented by R_t, can be separated into three core components (magnetic components, R_m) and a copper turns component, R_{Cu}. The components are

- frequency dependent eddy currents, R_F
- frequency dependent hysteresis, R_h
- magnetic drag, remanence loss, or residual loss, R_r
- copper winding loss including both dc and ac components, R_{Cu}, where

$$R_t = R_m + R_{Cu}$$
$$R_t = R_F + R_h + R_r + R_{Cu} \quad (\Omega) \qquad (17.26)$$

The coil is represented by the series R_t - L_s circuit where L_s is the lossless self-inductance. Empirical formulae, called *Jordan formulae* can be used to calculated R_t at low magnetic forces.

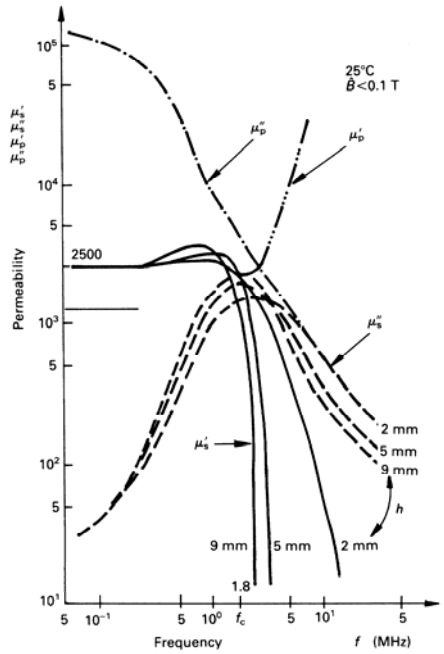

Figure 17.5. *Influence of core size (h) on the frequency characteristics of the complex permeability for a toroid.*

The series coil model impedance is given by

$$Z = R_t + j\omega L_s \qquad (\Omega) \tag{17.27}$$

whence

$$\begin{aligned}\tan\delta_t &= R_m + R_{Cu} \Big/ \omega L_s = R_t \Big/ \omega L_s \\ &= \frac{R_F}{\omega L_s} + \frac{R_h}{\omega L_s} + \frac{R_r}{\omega L_s} + \frac{R_{Cu}}{\omega L_s} \\ &= \tan\delta_F + \tan\delta_h + \tan\delta_r + \tan\delta_{Cu}\end{aligned} \tag{17.28}$$

where $\tan\ \delta_t$ is the loss factor for the coil. The reciprocal of the loss factor is the inductor quality factor, namely

$$Q = \frac{1}{\tan\delta_t} = \frac{\omega L_s}{R_t} \tag{17.29}$$

The copper loss is usually excluded so as to characterise the core material specifically, whence

$$Q = \frac{1}{\tan\delta} = \frac{\mu_s''}{\mu_s'} = \frac{\mu_p'}{\mu_p''} \tag{17.30}$$

An alternative core loss factor is $\tan\delta\ /\mu$ or $1/\mu Q$, which is generally characterised only for high frequency Ni-Zn ferrites. The loss factor for a gapped core, $\tan\ \delta_e$, can be found by multiplying the core loss factor by the gapped core effective permeability, μ_e, that is

$$\tan\delta_e = \frac{\tan\delta}{\mu}\mu_e \tag{17.31}$$

17.3.4ii - Core losses at high *H*

1 **- Ferrites**

Core losses, P_V, with high flux densities in Mn-Zn ferrites are applicable to power electronic application. Empirical formulae are not practical, and ferrites used for choke and transformer cores are provided with experimentally characterised total core loss per unit volume data, as indicated in figure 17.6. This loss, for a power Mn-Zn ferrite, is given as a function of frequency, temperature, and flux density.

For a specified and limited operating range, core losses in figure 17.6 can be approximated by

$$\begin{aligned}P_V\,(25°\text{C}) &= P_h + P_F \\ &= 5.8\times10^{-5}\times f^{1.2}\times\hat{B}^{2.11} + \ 3.32\times10^{-7}\times f^2\times\hat{B}^2 \qquad (\text{mW/cm}^3)\end{aligned} \tag{17.32}$$

where f is in kHz for 10 kHz $\le f \le$ 500 kHz

and $\hat{B}$ is the peak flux density in mT for 50mT $\le \hat{B} \le$ 250mT.

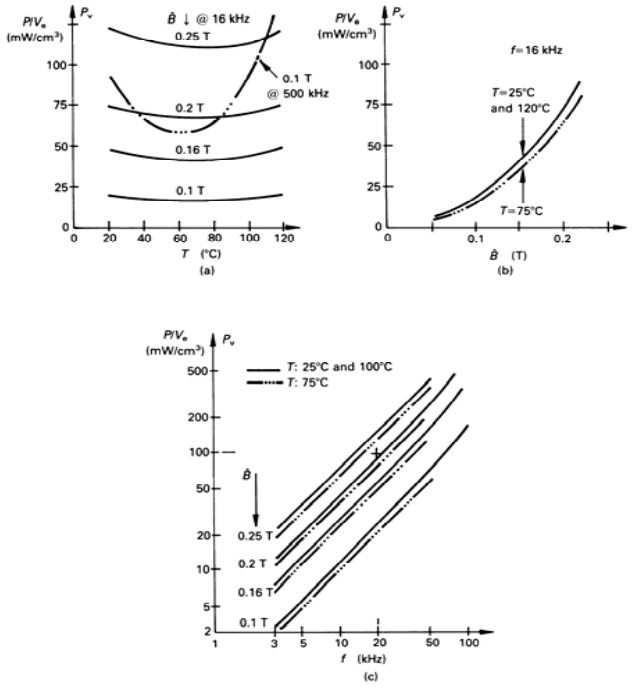

Figure 17.6. *Total per unit volume core losses as a function of: (a) core temperature, T; (b) maximum flux density, $\hat{B}$; and (c) frequency, f.*

Temperature dependence is modelled according to

$$P_V = \kappa \times P_V\,(25°\text{C}) \tag{17.33}$$

where

$$\kappa = 1.48\times10^{-4}\times T^2 - 21.2\times10^{-3}\times T\ + 1.44$$

for f < 200 kHz and $\hat{B} \ge$ 100 mT

$$\kappa = 1.2\times10^{-4}\times T^2 - 17.8\times10^{-3}\times T + 1.38$$

for $f \geq 200$ kHz and $\hat{B} \leq 100$ mT

where temperature T is with respect of 0°C.

The per unit volume loss $P_V(T)$ is applicable to a square wave. For a half wave sine, power losses are reduced by 0.7-0.8 while for a full wave rectified sine wave, losses are increased by 1.8 to 2.2.

2 - Laminated silicon steel

Hysteresis and eddy current losses for silicon steel can be calculated by using well established, classical empirical formulae.

(a) Hysteresis loss

Steinmetz equation predicts hysteresis loss according to

$$P_h = \lambda_h \hat{B}^n f V_e \quad \text{(W)} \qquad (17.34)$$

where λ_h and n are characteristics of the core

$n = 1.7$

$\lambda_h = 500$ for 4 per cent silicon steel

$= 3000$ for cast iron

(b) Eddy current loss

Eddy current loss is predicted by

$$P_F = \frac{\left(\pi \hat{B} f t\right)^2}{6\rho} V_e \quad \text{(W)} \qquad (17.35)$$

where t is the thickness of the lamination, parallel to the flux path, and ρ is the magnetic material resistivity. This formula illustrates why high resistivity ferrites have low eddy current loss, even at high frequencies. In the case of iron, the addition of 3-4 per cent silicon increases the resistivity by about four times, reducing both eddy current and hysteresis losses.

Eddy currents produce magnetic fields in the magnetic material, by Lenz's law, which will oppose the applied field. This reduces the flux density in the core centre such that most of the flux is confined to a thin layer or skin near the surface, termed *skin effect*.

Within a magnetic material with an ac flux, the flux density distribution is given by

$$B(x) = B(0)e^{\frac{-x}{\delta}} \quad \text{(T)} \qquad (17.36)$$

where x is the distance from the surface

$\delta = \sqrt{(\rho/\mu_o \pi f)}$ is called the skin depth.

Laminations should be less than $\frac{1}{2}\delta$ thick. The skin effect in metals can be used to absorb radiated and conducted rfi by using laminations $>2\delta$ thick.

A similar effect occurs within conductors carrying ac current, where the current is minimal at the conductor centre. The current density, J, is given by

$$J(x) = J(0)e^{\frac{-x}{\delta}} \quad (\text{A/m}^3) \qquad (17.37)$$

Below 20-50 kHz and above a few megahertz, solid wire is preferred. In between these frequencies, stranded wire, *Litz wire* (after *Litzendraht*) is preferred; decreasing from 0.07 mm to 0.03 mm in strand diameter as the frequency increases and interwinding capacitance dominates. Copper foil can also be employed.

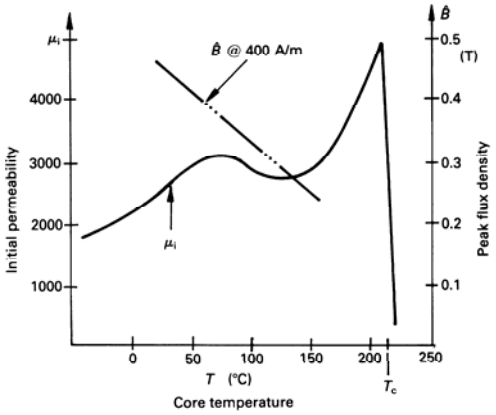

Figure 17.7. *Permeability, μ_i, and maximum density, $\hat{B}$, as a function of core temperature, T.*

17.3.5 Temperature effects on core characteristics

Generally ferrites have poor characteristic temperature stability. At higher temperatures, at the *Curie point*, cores lose their magnetic properties, abruptly. The phenomenon is reversible and below the Curie temperature, T_c, the material becomes magnetic again. The temperature effect on initial permeability in figure 17.7 illustrates the sudden loss of permeability at 212°C. Generally Curie temperature is inversely proportional to the initial permeability, μ_i. For most ferrites the initial permeability increases with temperature, and reaches a maximum just below the Curie temperature, as shown in figure 17.7.

Other ferrite parameters are also affected by temperature. Increased temperature decreases flux density and hysteresis loss as shown in figures 17.3 and 17.7. The effects of temperature on total core loss per unit volume are shown in figure 17.6a.

17.3.6 Inductance stability

Three factors affect inductance stability:

- *Parameter effects*
- *Time effects*
- *Temperature effects*

17.3.6i *- Parameter effects*

From the differential of equation (17.12)

$$\frac{dL}{L} = \frac{d\mu_e}{\mu_e} \tag{17.38}$$

while differentiating equation (17.16) yields

$$\frac{d\mu_e}{\mu_e^2} = \frac{d\mu_i}{\mu_i^2} \tag{17.39}$$

Substituting equation (17.39) into equation (17.38) gives

$$\frac{dL}{L} = \frac{d\mu_i}{\mu_i^2}\frac{A_L}{c} \tag{17.40}$$

The factor $d\mu_i / \mu_i^2$ is constant for a given temperature, hence any change in inductance is due to variations in A_L and c. Thus in order to increase the stability of an inductor in a given material with $\varepsilon << \ell_e$, it is necessary to increase the magnetic circuit air gap (to reduce the inductance factor A_L) or to select a bigger core (to increase the core permeance factor c).

17.3.6ii *- Time effects*

Initial permeability of a ferrite decreases with time under constant operating conditions, including constant temperature. A *disaccommodation factor*, *df*, independent of effective permeability, is introduced, which characterises the material such that the change in inductance is defined by

$$\frac{dL}{L} = df\ \mu_e \log_{10}\frac{t_1}{t_o} \tag{17.41}$$

This expression is based on the fact that permeability is proportional to the logarithm of time. The *df* increases slightly with temperature. Generally the *df* decreases, as shown in table 17.3:

- as the initial permeability increases for a given resistivity
- as resistivity decreases.

Example 17.1: ***Inductance variation with time***

A pot ferrite core with an effective permeability of 100 (A_L = 250) and a disaccommodation factor $df < 35 \times 10^{-6}$ has been in satisfactory operation for five weeks after production. What is the expected inductance variation after 10 years?

Table 17.3. Factors affecting the disaccommodation factor

			ρ(Ω cm)		
			10^5	500	≈ 20
μ_i			11-250	800-2000	4000
T_c		°C	450-300	250-170	145
df	× 10^{-6}		50-10	20-2	3

Solution

From equation (17.41)

$$\frac{dL}{L} = df\ \mu_e \log_{10}\frac{t_1}{t_o} < 35\times10^{-6}\times100\times\log\frac{520\text{ weeks}}{5\text{ weeks}}$$

that is, $dL < 0.7$ per cent can be expected.

♣

17.3.6iii *- Temperature effects*

Figure 17.7 shows that between +5°C and +55°C the permeability μ_i variation as a function temperature is approximately linear for this ferrite. The temperature coefficient α is given by

$$\alpha = \frac{1}{\mu_{i1}}\frac{\Delta\mu_i}{\Delta T} \qquad (\text{K}^{-1}) \tag{17.42}$$

where $\Delta\mu_i = \mu_{i2} - \mu_{i1}$ is the initial permeability variation over the temperature range $\Delta T = T_2 - T_1$.

In a magnetic circuit with an air gap and effective permeability, μ_e, the temperature coefficient of the core is reduced according to

$$\alpha_e = \alpha\frac{\mu_e}{\mu_i} = \alpha_F\mu_e \qquad (\text{K}^{-1}) \tag{17.43}$$

The term $\alpha_F = \alpha_i / \mu_i$ is called the relative temperature coefficient. The relative inductance change between two temperatures can be determined by

$$\frac{dL}{L} = \alpha_F\mu_e\Delta T \tag{17.44}$$

For effective permeability $\mu_e < 80$, the temperature coefficient $\alpha_e = \mu_e\alpha_F$ should be increased by 10 to 30 × 10^6/K to account for the temperature influence of the winding.

Example 17.2: ***Temperature effect on inductance***

The gapped pot core in example 17.1 is specified by a relative temperature coefficient of 1 x 10^6/K. What is the expected inductance variation over the temperature range 25-55°C?

Solution
From example 17.1

$$\mu_e = \frac{A_L}{c} = \frac{250}{2.5} = 100$$
$$\Delta T = 55 - 25 = 30°\text{C}$$

From equation (17.44)

$$\frac{dL}{L} = \alpha_F \mu_e \Delta T$$
$$= 1\times10^{-6}\times100\times30$$
$$= 0.3 \text{ per cent inductance variation}$$

♣

17.3.7 Stored energy in inductors

The energy stored in the magnetic field is given by

$$E = ½BH\breve{V}_e \quad \text{(J)} \tag{17.45}$$

where $\breve{V}_e$ is the effective minimum volume. It can be shown that the stored magnetic energy is equivalent to the stored electrical energy, whence

$$E = ½BH\breve{V}_e = ½Li^2 \quad \text{(J)} \tag{17.46}$$

For un-gapped cores, like a toroid, the ferrite effective volume, V_e, is equal to the minimum effective volume, $\breve{V}_e$. Inductors meeting this requirement may make the core size excessive. However the introduction of an air gap, ε, can reduce the core size significantly, since a significant amount of the energy can be stored in the gap volume. The minimum effective volume is now larger than the ferrite core effective volume, and is given by

$$\begin{aligned}\breve{V}_e &= V_e + A_e\mu_i\varepsilon \\ &= A_e\left(l_e + \mu_i\varepsilon\right) \quad (\text{m}^3)\end{aligned} \tag{17.47}$$

Figure 17.8 shows modified *B-H* characteristics for inductors with an air gap. The line curve o-b represents the core without an air gap, which results in the largest inductance. The energy stored in the core for a flux BA_e, in the linear portion of the curve, is the area of the shaded triangle 0-a-b, as defined by equation (17.45). When an air gap is introduced, the effective permeability falls as shown by the slope of line o-c. The figure

shows that as the air gap increases, the inductance decreases. It can be shown that the stored energy in the air gap and core is represented by the shaded area o-a-c, for a given flux, BA_e. It can be seen that the energy stored in the gap of length ε, although its length is much smaller than the core length, ℓ_c, its stored energy is much greater than that stored in the core.

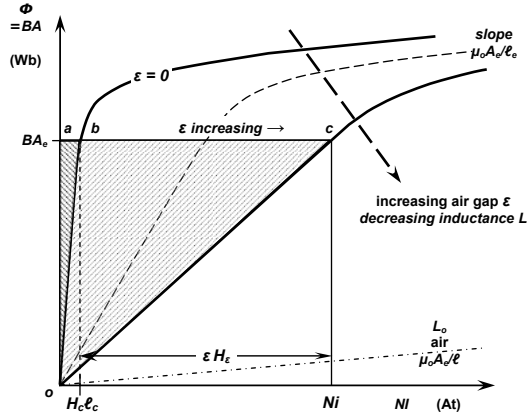

Figure 17.8. *Effects of air gap on inductance and stored energy.*

The total energy stored, E_T, in the magnetic circuit comprises the energy stored in the air gap, E_ε, plus the energy stored in the magnetic core material, E_{core}. It can be shown that these two energies are equal to the areas of the shaded triangles, o-b-c and o-a-b, respectively in figure 17.8. That is

$$\begin{aligned}E_T &= E_{core} + E_\varepsilon \\ &= ½B_cH_cV_c + ½B_\varepsilon H_\varepsilon V_\varepsilon\end{aligned} \tag{17.48}$$

If leakage is neglected, then the air gap flux is the same as the core flux. If fringing is neglected then the area of the core at the air gap is the same as the area of gap. Then

$$\begin{aligned}E_T &= ½BH_cA_e\ell_c + ½BH_\varepsilon A_e\,\varepsilon \\ &= ½BA_e\left(H_c\ell_c + H_\varepsilon\,\varepsilon\right)\end{aligned} \tag{17.49}$$

For a gapped core, as shown in figure 17.11

$$Ni = H_c\ell_c + H_\varepsilon\,\varepsilon \tag{17.50}$$

Therefore, on substituting equation (17.50) into equation (17.49) gives the total stored energy as

$$E_T = \tfrac{1}{2}BA_e\left(H_c\ell_c + H_\varepsilon\varepsilon\right) = \tfrac{1}{2}BA_e\left(Ni\right) \tag{17.51}$$

which is equal to the area of the shaded triangle o-a-b.
The inductance L is given by equation (17.4), that is

$$L = \frac{N\phi}{i} \tag{17.52}$$

Substitution of equation (17.50) for the current i gives

$$L = \frac{N^2\phi}{H_c\ell_c + H_\varepsilon\varepsilon} = \frac{N^2A_e\mu_o}{\frac{\ell_c}{\mu_r}+\varepsilon} = \frac{N^2A_e\mu_e}{\ell_c+\varepsilon}\left[\frac{\left(\ell_c+\varepsilon\right)\mu_r}{\ell_c+\mu_r\varepsilon}\right] = \frac{N^2A_e\mu_o\mu_e}{\ell_{total}} \tag{17.53}$$

where $\ell_{total} = \ell_c + \varepsilon$ and

$$\mu_e = \frac{\left(\ell_c+\varepsilon\right)\mu_r}{\ell_c+\mu_r\varepsilon} \tag{17.54}$$

Making the usual assumption that the length of the core is much greater than the length of the air gap, $\ell_c >> \varepsilon$, yields equation (17.18) for the effective permeability.

17.4 Ferrite inductor and choke design, when carrying dc current

Air gaps in magnetic circuits are introduced in order to reduce the influence of a superimposed dc current, manufacturing dispersion or to improve parameter stability. Saturable inductors for a semiconductor switch turn-on snubber normally do not employ an air gap, in order to reduce the stored energy, which may be subsequently dissipated, and to minimise the magnetising current magnitude.
Empirical equations have been derived for cylindrical inductors with a cylindrical core, which give an inductor with a large air gap. Design equations and examples are given in appendix 17.7.

17.4.1 Linear inductors and chokes

The introduction of an air gap reduces the effective permeability, μ_e such that the coil inductance is given by the equation (17.12)

$$L = \mu_e cN^2 = \mu_e L_o = A_L N^2 \qquad \text{(H)} \tag{17.55}$$

Figure 17.9a shows the variation of the effective permeability, μ_e at both low flux levels and without a dc bias, as a function of the relative air gap, ε/ℓ_e as specified by equation (17.17). As the air gap and the superimposed dc field are varied, the incremental permeability, μ_Δ varies as shown in figure 17.9b. This figure indicates how inductance varies with dc bias current (H).

Figure 17.9 does not specify the optimum inductor design since for a given inductance and dc current the optimum air gap and number of turns are not specified. The minimum number of turns and air gap requirements can be determined by means of the Hanna curves in figure 17.10.

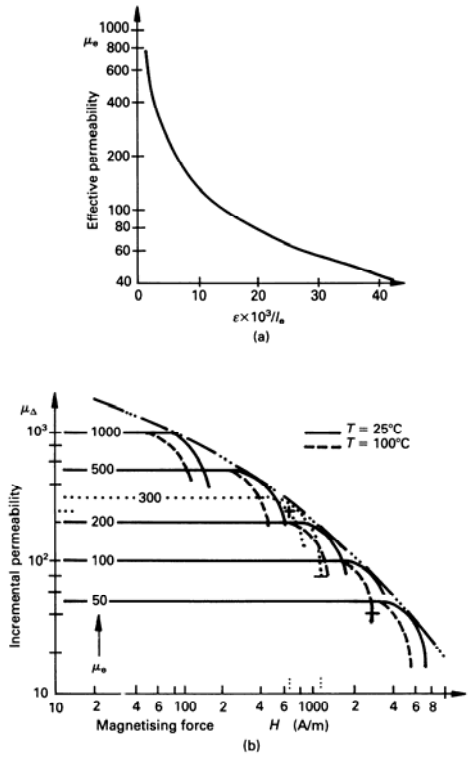

Figure 17.9. *Permeability as a function of:*
(a) air gap, ε and (b) superimposed dc field and air gap.

This figure shows experimental families of curves of per unit core energy against magnetomotive force per unit length, for different air gaps. The resultant curves are ferrite type dependent and dimensionally independent. Hanna curves therefore allow the determination of minimum turns N and air gap ε, from the required inductance L and dc current I.

Three distinct energy levels are shown in the Hanna curves in figure 17.10.

i. At low dc currents (H) the per unit energy increases linearly with H. This region corresponds to the horizontal regions in figure 17.9b, where

$$L = \mu_\Delta c N^2 \quad \text{(H)} \tag{17.56}$$

and as H varies, μ_Δ is constant.

ii. In the mid energy region, the per unit energy can decrease with increased H. The incremental permeability decreases, causing L to decrease at a greater rate than the increase in the dc current squared, I^2. This region is characterised by the fall off in μ_Δ, hence inductance, as H increases as shown in figure 17.9b.

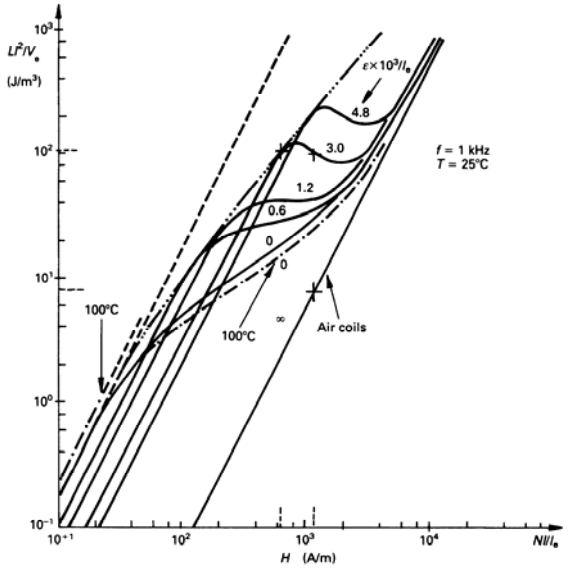

Figure 17.10. *Hanna curves, showing trajectories for different air gaps.*

iii. At high dc currents, the core material saturates, and μ_Δ tends to unity. An air core inductance results, where

$$L = L_o = c N^2 \tag{17.57}$$

Example 17.3: ***Inductor design with Hanna curves***

A 20 μH, 10 A choke is required for a forward converter. The inductance must be constant for unidirectional currents to 10 A. An available E-core pair has the following effective parameters

$\ell_e = 0.11$ m, $A_e = 175 \times 10^{-6}$ m^2, $V_e = 19.3 \times 10^{-6}$ m^3

and

$\mu_i = 2500$ @ 25°C and 3000 @ 100°C (from figure 17.7)

i. At a core temperature of 25°C, determine the required air gap and turns. Allow a 5 per cent decrease in inductance at rated conditions.

ii. Estimate the inductance at 20A dc.

iii. Calculate the inductance at 10A and 20A dc, both at 100°C.

Solution

i. Evaluate $\dfrac{LI^2}{V_e} = \dfrac{20\times10^{-6}\times10^2}{19.3\times10^{-6}} = 104$ J/m^3

From figure 17.10, restricted to the constant-L region, 104 J/m^3 corresponds to

(a) $\varepsilon/\ell_e = 3 \times 10^{-3}$

whence $\varepsilon = 3 \times 10^{-3} \times \ell_e = 3 \times 10^{-3} \times 0.11$

The required total air gap is 0.33 mm

(b) $H = 650$A/m

Since $H = NI/\ell_e$

$N = H\ell_e/I = 650 \times 0.11/10 = 7.15$ turns

Use 7 turns and a 0.33 mm total air gap.

ii. At 20 A, 25°C

$H = NI/\ell_e = 7 \times 20/0.11 = 1270$A/m

Two alternative design approaches may be used to estimate the inductance.

(a) The effective permeability, μ_e, before saturation can be evaluated from equation (17.17)

$$\frac{1}{\mu_e} = \frac{1}{\mu_a} + \frac{\varepsilon}{l_e} = \frac{1}{2500} + 3\times10^{-3}$$

that is

$$\mu_e \approx 300$$

From figure 17.9b, for μ_e = 300 it can be seen that the incremental permeability μ_Δ is constant, as required to 650A/m, then μ_Δ decrease as

saturation commences. At H = 1270A/m, μ_Δ has fallen to 75, from 300. The incremental inductance at 20 A is about ¼ of 20μH, namely 5.0μH.
(b) Alternatively, a simpler approach uses only figure 17.10. H = 1270A/m projects 100 J/m^3. Solving $100.0 = L_{20A} I^2/V_e$ with I = 20A yields L_{20A} = 5μH.

iii. The effective permeability at 100°C is

$$\frac{1}{\mu_e} = \frac{1}{\mu_i} + \frac{\varepsilon}{l_e} = \frac{1}{3000} + 3\times10^{-3}$$

that is

$$\mu_e \approx 300$$

It is seen that, although the initial permeability varies significantly with temperature, here the effective permeability is dominated by the air gap, and hence is essentially temperature independent. Figure 17.9b, with H = 640A/m, projects μ_Δ = 220 at 100°C. Using $L\ \alpha\ \mu_\Delta$, the inductance falls to about 15μH at 100°C, 10 A.
At 20A, 100°C, the effects of saturation are highly significant, and figure 17.9b indicates that the incremental permeability is low. The best approximation is to use the air coil curve in figure 17.10. Hence H = 1270A/m projects 9J/m^3. At 20A, 100°C, an inductance of at least 0.43μH can be expected.

♣

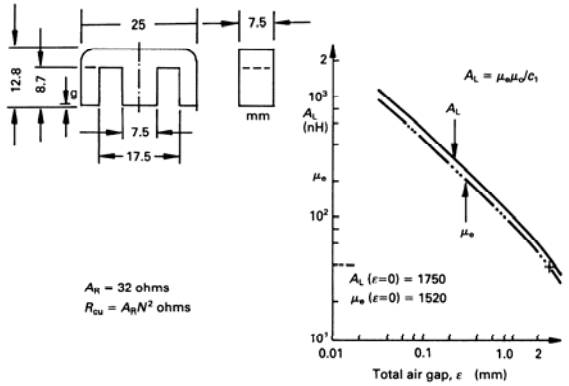

Figure 17.11. *Characteristics of a pair of gapped E-cores. Core dimensional parameters are given in table 17.5.*

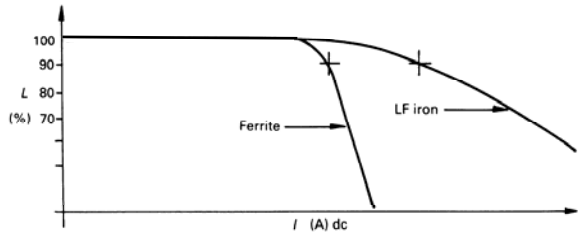

Figure 17.12. *Comparison of inductance characteristics illustrating how inductance falls off faster with ferrite cores than with iron cores, at higher currents.*

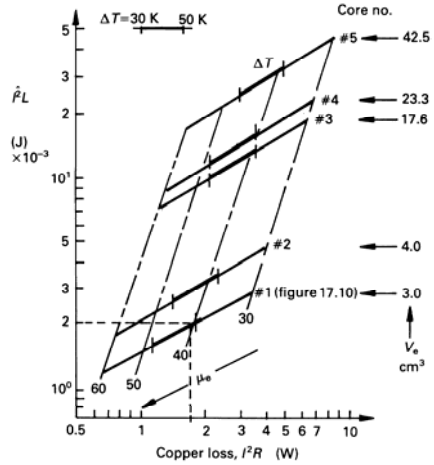

Figure 17.13. *Magnetic biasing capability $\hat{I}^2L$, copper loss I^2R, effective permeability μ_e and over-temperature ΔT of five different effective volume V_e ferrite cores.*

Figure 17.4 shows how μ_Δ and hence the inductance, falls off as H, and hence the current, increases for ferrite core materials. The larger the air gap, and hence the lower A_L, the higher H before inductance rolls off. Inductance rolls off faster, the wider the air gap, hence the higher the magnetic field strength, H. The decrease in effective permeability, μ_e and inductance factor, A_L, with increase of air gap, ε, is shown in figure 17.11 for two E-cores.

Figure 17.12 shows typical curves for the decrease in μ_Δ, hence inductance, with increased H, hence current, for both ferrites and alloy or iron powder cores. Because power ferrites have a squarer B-H curve than powder cores, the inductance of ferrites falls off faster. By increasing the core volume, the fall off rate of inductance can be reduced. Depending on core loss for a given volume, a powder core may be more effective than a ferrite; and would have better utilisation of the copper window area. The design approach previously considered in example 17.3 in fact neglects the optimisation of core size and copper I^2R loss.

17.4.Ii - Core temperature and size considerations

Figure 17.13 relates stored energy, LI^2, and copper loss, I^2R, for different cores of the same ferrite type. Once L and I are fixed, figure 17.13 can be used to determine the optimum core size and air gap. This figure shows that with increasing air gap (decreasing μ_e), the magnetic biasing capability increases along with the associated copper loss, I^2R. A flowchart is shown in figure 17.14, which outlines the design procedure to be used in conjunction with figure 17.13.

Example 17.4: ***Inductor design including copper loss***

With the aid of figure 17.13, design a 20 μH, 10 A dc inductor, calculating the copper loss and temperature rise for the predicted optimum air gap and number of turns.

Solution

Following the procedure outline in the flowchart of figure 17.14

Evaluating $LI^2 = 20 \times 10^{-6} \times 10^2$

$= 2$ mJ

From the nomogram in figure 17.13 use core no. 1, which must have $\mu_e = 40$ and $I^2R = 1.8$ W. This copper loss will produce a 50°C temperature rise above ambient on the core surface, beneath the winding. The thick bars in figure 17.13 represent a 30-50°C temperature increase range.

The core type no. 1 has A_L and μ_e values versus total air gap, and effective parameters as shown in figure 17.11 and table 17.5. For $\mu_e = 40$, $A_L = 45$ nH, a total air gap of 2.7 mm is required.

From $L = A_L N^2$

$N = \sqrt{20 \times 10^3/45}$

$= 21$ turns

For $I = 10$ A dc, $I^2R_{Cu} = 1.8$ W, then $R_{Cu} = 18$ mΩ. The copper turns diameter is determined from

$$R_{Cu} = N \ell_N R_L \quad (\Omega) \tag{17.58}$$

where R_L is the resistance per meter, Ω/m

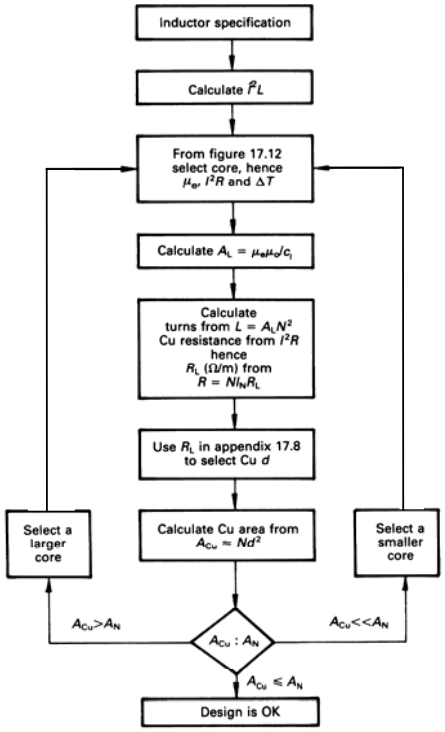

Figure 17.14. *Linear inductor design flowchart.*

ℓ_N is the mean turn length which is either provided for a given former or may be estimated from core physical dimensions. From table 17.5:

$$\ell_N = 52 \text{ mm}$$
$$R_L = R_{Cu} / N\,\ell_N$$
$$= 18 \times 10^{-3}/21 \times 52 \times 10^{-3} = 0.165\ \Omega/\text{m}$$

Using standard wire tables, appendix 17.9 for 0.165 Ω/m, use 28 SWG (0.154 Ω/m) which has a diameter of 0.36 mm and 0.434 when enamelled. The resultant copper current density is 77 A/mm^2. In many applications 4 A/mm^2 is used for finer gauge wires up to 20 A/mm^2 for heavier gauge wires. These current densities represent about 5 per cent of the fusing current , I_{fusing} which is approximated by

$$I_{\text{fusing}} = 80\,d^{1.5}$$

The diameter d is in mm.

This recommendation is unrealistic and inductor and transformer design is based on temperature rise.

The approximate copper area is

$$A_{Cu} = N \times d^2$$
$$= 21 \times 0.434^2$$
$$= 3.88\text{mm}^2$$

From table 17.5, the useful winding cross-section is

$$A_N = 56 \text{ mm}^2$$

Only 8 per cent of the former window area is filled, hence the actual copper length is overestimated and I^2R loss, hence temperature rise, will be less than the allowed 1.8 W and 50°C respectively.

♣

Comparing the design of examples 17.3 and 17.4, it will be seen that the same design specification can be fulfilled with the latter core of 20 per cent the volume of the former. The bigger core required an 0.33 mm air gap to give μ_e = 300, while the smaller core required a larger gap of2.7 mm to give μ_e = 40. Both cores are of the same ferrite type. The incremental inductance of the smaller core will fall off with current, much faster than with the larger core, as indicated by figure 17.4.

For a switch mode power supply application, the rms value of current is less than the peak current at which the inductance is specified. The copper loss, hence temperature rise, is then based on an rms current basis.

17.4.2 Saturable inductors

Saturable inductors are used in series with semiconductor switching devices in order to delay the rise of current, thereby reducing switch turn-on stress and loss. In the case of a power transistor, the collector current is delayed until the collector voltage has fallen (see 8.3.4). For thyristor devices, the delay time allows the gate activated cathode area

to spread hence giving a high initial di/dt capability. In each case the inductor supports the supply voltage, then after a finite time saturates to a very low inductance, supporting little voltage, and does not influence the switch current.

Ferrites are ideal as the core of a saturable inductor because of their low magnetic field strength, H_s, at the onset of flux density saturation, B_s. While the inductor supports voltage, v, the flux density increases, moving up the B-H curve according to Faraday's law

$$v = NA_e \frac{dB}{dt} \tag{17.59}$$

A low magnetising current results. After a finite time the flux density reaches the knee of the B-H curve (B_s, H_s), the core saturates and the incremental permeability falls from an initially high value to that of air, μ_Δ = 1. The high initial permeability, hence high inductance, limits the current. The time t_s, for the core to saturate should be equal to the switch voltage fall time, t_{fi}. The low saturation inductance allows the switch current rapidly to build up to a level dictated by the load.

If the switch voltage fall is assumed linear then the inductor voltage is $V_s\,t/t_{fi}$. The time t_s, taken to reach saturation (B_s, H_s) from integration of Faraday's law is

$$t_s = \frac{2NA_eB_s}{V_s} \tag{17.60}$$

for $t_s \le t_{fi}$.

The flux density, hence H, and current increase quadratically with time. At saturation the magnetising current magnitude (hence switch current) is

$$I_s = \frac{H_s\ell_e}{N} \quad \left(= \frac{2B_sH_sV_e}{t_sV_s}\right) \quad \text{(A)} \tag{17.61}$$

which should be small compared with the switch on-state current magnitude.

The inductance before saturation is given by

$$L = A_L N^2 \quad \text{(H)} \tag{17.62}$$

and falls to

$$L_{sat} = c\,N^2 \quad \text{(H)} \tag{17.63}$$

after saturation, when leakage and lead length will, in practice, dominate inductance.

The energy stored in the core and subsequently dissipated at core reset is given by

$$E = \tfrac{1}{2}B_sH_sV_e \quad \left(= \tfrac{1}{4}I_sV_st_s\right)$$
$$= \tfrac{1}{2}B_sH_sA_e\ell_e \quad \text{(J)} \tag{17.64}$$

which must be minimised.

Table 17.4 summarises saturable inductor requirements based on equations (17.60) to (17.64).

Table 17.4. Design requirement of a saturable inductor

	Material dependent		Shape dependent		
	H_s	B_s	A_e	ℓ_e	N
Minimise E $E = ½ B_s H_s A_e \ell_e$	low	low	low	low	×
Maximise t_s $t_s = 2NA_eB_s/V_{sec}$	×	high	high	×	high
Minimise I_s $I_s = H_s\ell_e/N$	low	×	×	low	high
Maximise L $L_a = N^2A_eB_s/\ell_eH_s$	low	high	high	low	high
Requirement	low H_s (high μ_r)	-	-	short ℓ_e	high N
Compromise	-	high B_s if H_s is low	high A_e if ℓ_e is short		

17.4.3 Saturable inductor design

Figure 17.15 shows a saturable inductor design flowchart. The design starting point is the type of ferrite. The desired ferrite should have minimal high frequency loss, associated with a small magnetic field strength, H_s, at saturation. These features would be associated with ferrites having a low coercive force, H_c and remanence, B_r. The ferrite material shown in figure 17.3 fulfils these requirements with

$$H_c = 12\text{A/m} \qquad B_r = 0.18\text{T}$$
$$H_s = 200\text{A/m} \qquad B_s = 0.4\text{T}$$

Ferrites with lower magnetic field strengths are available but tend to be limited in size.
A material with a high initial permeability is one indicator of a suitable ferrite type.
The next considerations are core shape and effective core parameters such as effective length, ℓ_e and area, A_e. The core should have a short effective length, ℓ_e. The area and length are traded in maintaining sufficient copper window area, A_N.
A core shape without an air gap will produce the highest possible initial, hence effective, permeability. Example 17.5, which follows, illustrates that a toroid core offers a good solution.
A high number of turns, N, is desirable, and preferred to an increase in area, A_e.
Design should be based on the maximum core temperature. An increase in temperature decreases H_s at a faster rate than B_s, as shown in figure 17.3. From equation (17.60), many turns are required which, in combination with decreased H_s, advantageously decrease the magnetising current, I_s.

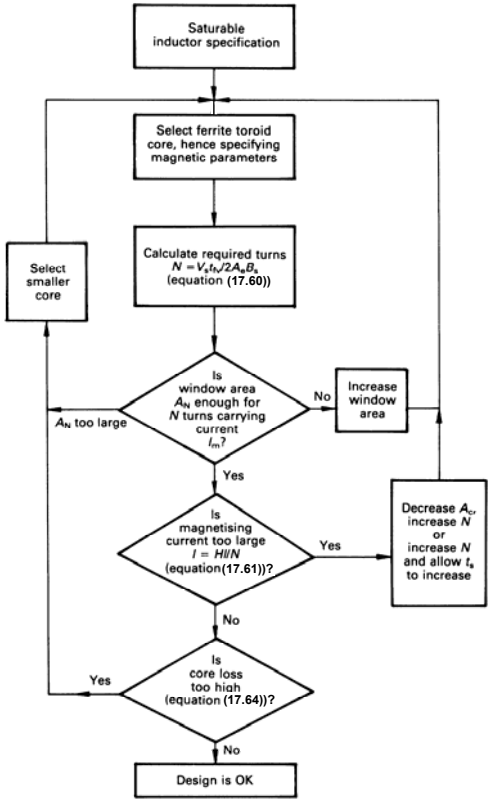

Figure 17.15. *Saturable inductor design flowchart.*

Table 17.5. Pot, toroid, and E-core design data.
Applicable magnetic data are presented in appendix 17.8

		Physical dimensions (mm)		
		Pot core d_o = 25 h = 16	Toroid d_o = 39 d_i = 24.77 h = 6.61	E-core (pair) See figure 17.11
V_e	cm^3	3.63	3.86	3.02
A_e	cm^2	0.999	0.398	0.525
ℓ_e	cm	3.64	9.71	5.75
c_1	cm^1	3.64	24.4	10.9
A_{min}	cm^2	0.95	0.398	0.45
A_L	nH	4300	1540	(ε = 0)1750
μ_e		1245	(μi) 3000	(ε = 0)1500
c	nH	3.45	0.51	1.15
A_N	cm^2	0.357 (0.266)	4.75	0.56
ℓ_N	cm	5.3 (5.35)	7.6	5.2
S_A	cm^2	18.4	48.7/58	20
Weight	g	23.4	19.3	2 × 8

Example 17.5: ***Saturable inductor design***

A pot, toroid and E-shaped core of the same Mn-Zn ferrite as characterised in appendix 17.8, and of similar volume, have characteristics and parameters as shown in table 17.5, with H_s = 200At/m.
Design a saturable inductor for each core shape, for a switch having a 200 ns linear voltage fall time and operating on a 600 V dc supply rail.
The core is to saturate when the switch voltage reaches saturation (0 V).
Estimate the core power removed at reset if the switching frequency is 20 kHz.

Solution

		Pot	Toroid	E-cores (ε = 0)
From equation (17.60) $N = V_s t_{fv}/2A_eB_s = 1.875/A_e$ A_e is in cm^2		2	5	4
From equation (17.61) $I_s = H_s\ell_e/N = 2\ell_e/N$ ℓ_e is in cm	(A)	3.64	3.85	2.83
From equation (17.62) $L = A_L N^2 \times 10^{-3}$	(μH)	17.2	38.5	28.0
From equation (17.63) $L_{sat} = cN^2$	(nH)	13.8	12.75	18.4
From equation (17.64) $P_d = V_e \times 8 \times 10^{-1}$ V_e is in cm^3	(W)	2.90	3.09	2.42

Based on the available copper window area, A_N and number of turns, the cores would be applicable to switching currents in excess of 100 A. Smaller cores could be used for lower current levels, although A_N tends to dictate the required core.
From equation (17.64), the power dissipated at 20 kHz is given by $P_d = \frac{1}{2}B_s H_s V_e f_s$.

♣

17.5 Power ferrite transformer design

A Mn-Zn ferrite material is almost exclusively used for power transformer cores, and has been optimised by manufacturers for a wide frequency range. Specific core shapes have also been developed to cover a wide power range. In the case of voltage transformers, at 20 kHz and below 100 W, pot cores are used, or when low flux leakage and low emi are important. Such cores can be processed on automatic machines which wind and assemble the whole unit. At powers above 100 W, E-E and E-I cores are extensively used.
The usable power range of the pot core is increased by increasing frequency and at 500 kHz no alternative exists, because of the low leakage flux, low self-capacitance, and good shielding offered by pot cores.

17.5.1 Ferrite voltage transformer design

To simplify ferrite core selection, manufacturers provide the characteristic curves given in figure 17.16 which show the power that can be transmitted by various core shapes. Specifically, these curves show power for the modes of operation commonly used in switch-mode power supplies; such as push-pull, forward, and flyback, as considered in

chapter 15, versus the core plus copper volume.
A formal transformer design approach based on copper and core losses is shown in the flowchart in figure 17.17 and is applicable to all smps types.

Stage 1 and stage 2

The transformer, primary and secondary voltages, currents, and powers, hence efficiency, must be specified or determined. Other requirements are frequency, ambient temperature, and allowable temperature rise at the core to copper interface. The final specification should include

$$\begin{matrix} V_p & V_s \\ I_p & I_s \\ P_p & P_s \end{matrix} \qquad \eta, f, T_a, \Delta T$$

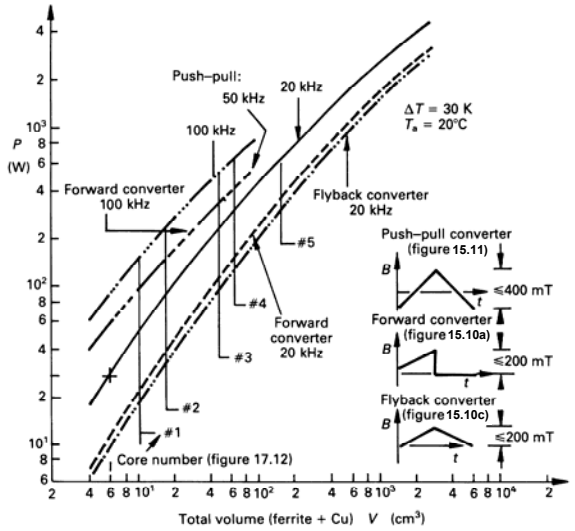

Figure 17.16. *Transmissible power, P, versus volume (ferrite plus copper), V, of transformers with ferrite Mn-Zn cores.*

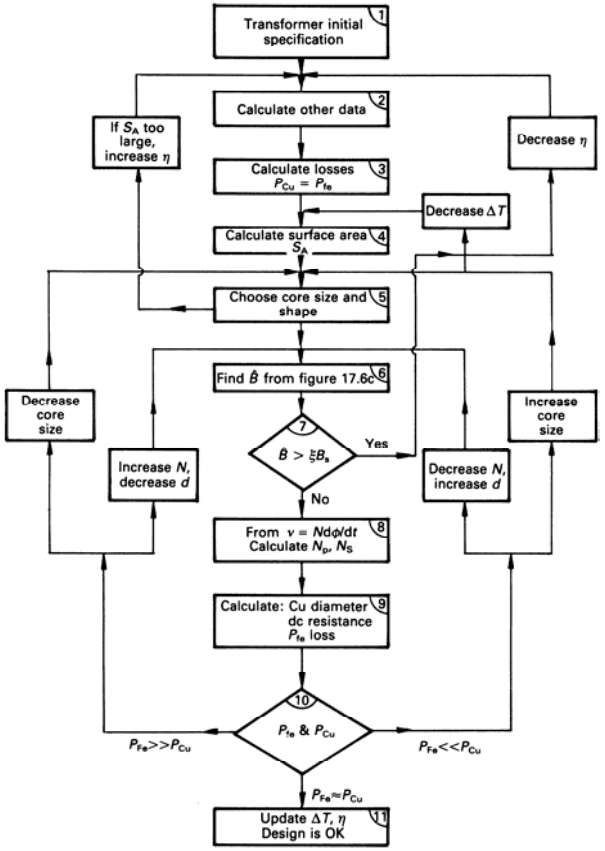

Figure 17.17. *Voltage transformer design flowchart.*

Stage 3

The difference between input power and output power is the total power loss, P_L, which comprises copper and core losses. The maximum efficiency is obtained when the copper loss equals the core loss.

Stage 4

The total power loss, P_L, ambient temperature, T_a, and temperature rise, ΔT, specify the exposed copper and core surface area requirements, S_A, according to (see equation 5.4)

$$S_A = \frac{P_L}{\Delta T\, S_d} \quad (\text{m}^2) \tag{17.65}$$

where S_d is a surface dissipation factor.
Empirical equations are commonly provided for S_d. Based on the assumption that thermal stability is reached half by convection and half by radiation, the surface area requirement can be approximated by

$$S_A = 145 \times \left[\frac{1000}{T_a + 273}\right]^{2.06} \frac{P_L}{\Delta T^{1.22}} \quad (\text{cm}^2) \tag{17.66}$$

Stage 5

A core with the minimum surface area, S_A, is selected using manufacturers' data, ensuring that the ferrite type is appropriate to the operating frequency and that the core shape meets any engineering, cost or other special requirements. The manufacturers' data required include the effective dimensional parameters, copper winding area, A_N, and average turn length, ℓ_N.
Some manufacturers provide transformer design data for each core. This specific data can be employed, rather than the general procedure that follows.

Stage 6

Using the core volume, V_e, and core loss $P_c = ½P_L$, whence core loss per cm^3, $P_w = P_c / V_e$ the maximum allowable operating flux density, B_{op}, for the specified frequency can be determined from the power loss curves in figure 17.6c.

Stage 7

The rated saturation flux density, B_s, cannot safely be used. For a transformer using both quadrants of the *B-H* characteristics, for example, a push-pull smps transformer

$$B_{op} \le 0.8\, B_s$$

while for a core used with a flux bias

$$B_{op} \le 0.4\, B_s$$

These limits avoid operational saturation of the core in one direction. If the working flux density, B_{op}, is too high, either

- reduce the efficiency and go to stage 1/2, or
- reduce the allowable temperature rise and go to stage 4.

Stage 8

The required number of primary turns, N_p, can be calculated from Faraday's law, which yields

$$N_p = \frac{V_p}{k\, B_{op} A_e f} \tag{17.67}$$

where $k = 4$ for a square-wave voltage
$k = 4.44$ for a sine wave.
If $B_{op} > 100$ mT, the effective area, A_e, in equation (17.67) is replaced by the core minimum area section, A_{min}, since that portion experiences the highest flux density.
The number of secondary turns is calculated according to

$$N_s = N_p \frac{V_s}{V_p} \tag{17.68}$$

Stage 9

The winding diameter, d_p, for the allotted primary for a window area, A_p, is calculated according to

$$d_p = 2\sqrt{\frac{A_p k_w}{\pi N_p}} \quad (\text{m}) \tag{17.69}$$

where k_w is a winding space factor, 0.7, which accounts for insulation, winding taps, shielding, air space, etc. A similar expression for the diameter of the secondary, d_p, involves the number of secondary turns, N_s, and allotted area, A_N. The total winding area $A_p + A_s$ must not exceed the available winding area, A_N.
Standard copper wire tables, appendix 17.9, provide the resistance per meter, R_L, for the calculated diameters. From equation (17.58), the dc resistance of the primary can be calculated according to

$$R_p = N_p\, \ell_N\, R_{Lp} \quad (\Omega) \tag{17.70}$$

Similarly for calculating the secondary dc resistance, R_s. The total copper loss can be calculated as

$$P_{Cu} = I_p^2 R_p + I_s^2 R_s \quad (\text{W}) \tag{17.71}$$

Stage 10

The core loss, P_c, and the copper loss, P_{Cu} are compared. If

(i) $P_{Cu} > P_c$

Either decrease the number of turns and increase the copper diameter. This will reduce the copper loss and increase B_{op}, and hence P_c. Recalculate from stage 6.

or select a larger core, which will increase the copper window area, A_N, hence increasing the allowable wire diameter. Recalculate from stage 5.

(ii) $P_{Cu} < P_c$

Either increase the number of turns which will reduce d, B_{op} hence P_c, and then recalculate from stage 6.

or select a smaller core, which will require d to be reduced, and then recalculate from stage 5.

Proceed if $P_{Cu} \approx P_c$.

Stage 11

Update the value of total losses, P_L, and hence recalculate the power requirements and resultant efficiency.

Calculate the actual core temperature rise from equation (17.66), rearranged

$$\Delta T = 59\left(\frac{1000}{T_a + 273}\right)^{1.69} \times \left(\frac{P_L}{S_A}\right)^{0.82} \quad \text{(K)} \qquad (17.72)$$

where S_A is the heat dissipating area in cm^2 of the chosen core.

Example 17.6: ***Ferrite voltage transformer design***

Consider the design requirements for the split rail push-pull smps shown in figure 15.7b, which is specified as follows

$v_o = 5$ V — $V_{sec} = 48$ V ± 15 per cent
$i_o = 4$A — $f = 20$kHz
$P_o = 20$ W — $T_a = 25$°C, $\Delta T \leq 35$ K
$\eta = 97$ per cent

Solution

Based on the flowchart in figure 17.17 and the eleven stages outlined, design proceeds as follows.

Stage 1

The transformer must deliver 20 W plus losses associated with an output inductor and the pair of Schottky diodes in the output rectifier. The inductor loss is estimated at 4 per cent of the output power, 0.8 W, while the diode total loss is 0.6 V × 4 A = 2.4 W. Thus the transformer output power requirement P_s is 23.2 W (20 W + 0.8 W + 2.4 W). With a 97 per cent efficiency, the transformer input power, P_p, requirement is 1/97 per cent of 23.2 W, namely 23.9 W. The nominal primary current, I_p, at the nominal voltage, 24 V is

$$I_p = \frac{P_p}{V_{pn}} = \frac{23.9\text{W}}{24\text{V}} = 1\text{A}$$

The maximum primary voltage, V_p, is $1.15 \times V_{sec}/2 = 27.6$ V, since the 48 V supply is centre tapped and has + 15 per cent regulation. For worst case, it is assumed that the voltage drop across the switches is zero.

The transformer secondary voltage, V_{sec}, for the centre tapped full-wave rectifier circuit, must be large enough to overcome the diode voltage drop, V_d, and must allow for averaging of the nominal low duty cycle switching action of the primary input power. With pwm regulation each input switch operates for approximately 25 per cent of the time, thus

$$\tfrac{1}{2}V_s = 2 \times (V_o + V_d)$$

where the ½ indicates that half of the secondary winding conducts at any one time, while the 2 approximates the pwm average on-time. Thus for $V_d = 0.6$ V and $V_o = 5$ V

$$V_{sec} = 4 \times (5 + 0.6) = 22.4\text{V}$$

Stage 2

Extracting the transformer data from stage 1

$I_p = 1$A — $I_s = 4$A
$V_p = 27.6$ V — $V_{sec} = 22.4$ V
$P_p = 23.9$ W — $P_s = 23.2$ W

$\eta = 97$ per cent, $f = 20$ kHz, $T_a = 25$°C, $\Delta T = 35$ K

Stage 3

The total transformer power loss, P_L, from $P_s - P_p$, is 0.7 W.
Thus $P_c = P_{Cu} = 0.7/2 = 0.35$ W each.

Stage 4

The surface area requirement is calculated from equation (17.66)

$$S_A = 145 \times \left[\frac{1000}{25 + 273}\right]^{2.06} \times \frac{0.7\text{W}}{35^{1.22}}$$

$= 16.1$ cm^2 for a 35 K temperature rise

Stage 5

Either the pot core in table 17.5 or the pair of E-cores in figure 17.11 have sufficient surface area, 18.4 and 20 cm^2 respectively, and both are of a ferrite material suitable for a 10 to 100 kHz operating frequency range.
At the low power level of 23.9 W, choose the pot core.

Stage 6

Using the technical data given in table 17.5, the core loss per unit volume is calculated

$$P_w = \frac{P}{V_e} = \frac{0.35\text{W}}{3.63\text{V}} = 0.096\text{W/cm}^3$$

Stage 7

From figure 17.6c, an operating flux density of 0.21 T at 20 kHz will result in the allowable core loss of 0.1 W/cm^3. For push-pull operation the maximum allowable flux density is about 80 per cent of B_s, that is, 80 per cent of 0.48 T, namely 0.38 T. Since 0.21 T < 0.38 T, a working flux density of 0.21 T is acceptable.

Stage 8

Since the operating flux density is greater than 100 mT, the pot core minimum area, A_{min} (0.95 cm^2) is used for calculations, rather than the effective area, A_e (0.999 cm^2). From equation (17.67), the required number of primary turns is given by

$$N_p = \frac{27.6\text{V}}{4 \times 0.21\text{T} \times 0.95 \times 10^{-4} \times 20 \times 10^3} = 17.3$$

Use 17 turns.
The number of secondary turns is given by equation (17.68)

$$N_s = \frac{22.4}{24} \times 17 = 15.7$$

where the nominal primary voltage is used. Use 16 turns per secondary winding.

Stage 9

From table 17.5, the available winding area, A_N, is either 0.357 cm^2 for a one-section former or 0.266 cm^2 for a two-section former. Since the primary and secondary voltages are relatively low, insulation and isolation present few difficulties, hence single enamel copper wire and a single section former can be used. The available copper area, 0.357 cm^2, is divided between the primary and secondary so as to provide a uniform current density within the winding area. The primary to secondary currents are in the ratio of 1:4, hence 0.285 cm^2 is allocated to the secondary (approximately 80 per cent) while 0.072 cm^2 is allocated to the primary winding. The copper wire diameter is calculated using equation (17.69)

$$d_p = 2\sqrt{\frac{A_p k_w}{\pi N_p}} = 2 \times \sqrt{\frac{0.072 \times 10^{-4} \times 0.8}{17\pi}} = 0.66 \text{ mm}$$

$$d_s = 2\sqrt{\frac{A_s k_w}{\pi N_s}} = 2 \times \sqrt{\frac{0.285 \times 10^{-4} \times 0.8}{32\pi}} = 0.95 \text{ mm}$$

Using the standard wire tables in appendix 17.9 and equation (17.58) to calculate the winding resistance

		Primary	Secondary	
d_{Cu}	mm	0.6	0.95	bare Cu
d_{Cu+en}	mm	0.65	1.017	single enamel
R_L	Ω/m	0.06098	0.02432	
R_{Cu}	Ω	0.055	0.0206/16 turns	

The total power copper loss is given by equation (17.71)

$$\begin{aligned} P_{Cu} &= I_p^2 R_p + I_s^2 R_s \\ &= 1^2 \times 0.055 + 4^2 \times 0.0206 \\ &= 0.055 + 0.330 = 0.385\text{W} \end{aligned}$$

Stage 10

The core loss is 0.35 W while the copper loss is only slightly higher at 0.385 W. No iterative change is necessary. The updated total loss, P_{L_s} is 0.735 W.

Stage 11

The secondary power requirement remains 23.2 W while the primary requirement has increased to 23.94 W. The efficiency has been reduced to

$$\eta = \frac{23.3\text{W}}{23.94\text{W}} \equiv 96.9\,\text{per cent}$$

from 97 per cent.
Using the actual core surface area, 18.4 cm^2, and loss, 0.735 W, the core temperature rise can be calculated from equation (17.72)

$$\begin{aligned} \Delta T &= 59 \times \left(\frac{1000}{25+273}\right)^{1.69} \times \left(\frac{0.735}{18.4}\right)^{0.82} \\ &= 32.6 \text{ K} \end{aligned}$$

which is less than the 35 K allowable temperature rise limit.

♣

The transformer design of example 17.6 could be based on figure 17.16. The volume of the core plus copper, for the pot core in table 17.5, can be estimated from its diameter of 25 mm and height of 16 mm. This yields a total volume of 6 cm^3, after allowing for slots.
Using figure 17.16, for a total volume of 6 cm^3, at 20 kHz, for a push-pull converter, 28 watts can be transmitted in a 20°C ambient, producing a 30 K core temperature rise. These results and those from example 17.6 compare as follows.

		Figure 17.16	Example 17.6
P	W	28	23.2
ΔT	K	30	32.6
T_a	°C	20	25

All other operating conditions are identical. Any design discrepancy is accounted for by

- the higher ambient temperature
- the poorer winding slot utilisation.

A centre tapped secondary represents poorer slot utilisation compared with using a single winding, which requires four rectifying diodes since, because of a limited core size range, the same core would be used independent of the type of secondary circuit. A centred tapped secondary would result in the cost saving associated with two fewer Schottky diodes.

17.5.2 Ferrite current transformer

By adding a secondary winding, a linear inductor can be converted into a voltage transformer, while a saturable inductor can be converted into a current transformer. The linear inductor and voltage transformer (of E-I laminations) are characterised by a core with an air gap (inherent in transformers which use E-I laminations). The saturable inductor and current transformer generally use an un-gapped core.
A given transformer can operate either in the voltage mode or the current mode depending on the load impedance. The voltage transformer operates into a high impedance circuit, while the current transformer requires a low impedance load. Current and voltage transformer action both cease at core saturation.
The equivalent circuit model is identical for each transformer mode, and the same basic equations apply in each case. A saturable inductor is required to support a large voltage for a short period, while a current transformer supports a low voltage for a long period. In each case, the primary voltage-time product is equal for a given core and primary turns.

17.5.3 Current transformer design requirements

The basic requirement of a current transformer is a fixed ratio between the primary and secondary currents according to

$$I_p N_p = I_s N_s \quad \text{(A)} \tag{17.73}$$

Ideally the load impedance is zero, hence zero secondary voltage is developed. Practically, a secondary voltage, V_{sec}, exists, whence from Faraday's law

$$V_{sec} = N_s \frac{d\phi}{dt} = N_s A \frac{dB}{dt}$$

For a constant secondary voltage (a short circuit), the core flux density increases linearly, effectively moving up the *B-H* curve and reaches saturation, B_s, in time

$$t_s = \frac{N_s B_s A_e}{V_{sec}} \quad \text{(s)} \tag{17.74}$$

Where a core is operated with an *H* offset, for example, as with an inductor carrying dc current or a unidirectional current transformer, the maximum value of flux density used for analysis should be reduced because of remanence to B_s - B_r, whence

$$t_s = \frac{N_s \left(B_s - B_r\right) A_e}{V_{sec}} \quad \text{(s)} \tag{17.75}$$

The lower the secondary voltage, V_{sec}, the longer the time before saturation, at which point current transformer action ceases. The core is fully reset by a negative voltage of sufficient duration for which the voltage-time product must equal that of the on-period. Fortunately, a high reset voltage can generally be employed, which produces a very short reset time. Effectively, the reset voltage forces the magnetising current, or stored energy, to zero.
This magnetising current, $\check{I}_P$ should be minimal and its presence modifies the ideal ampere-turns balance according to

$$\left(I_p - \check{I}_p\right) N_p = N_s I_s \quad \text{(A)} \tag{17.76}$$

where the magnetising current $\check{I}_P$ is given by

$$\check{I}_p = \frac{H \ell_e}{N_p} \quad \text{(A)} \tag{17.77}$$

The initial magnetising current is zero, and increases linearly with time. Low leakage core shapes should be used to minimise leakage inductance.
At all times the primary voltage is related to the secondary voltage according to

$$V_p = V_{sec}\left(\frac{N_p}{N_s}\right) = \frac{V_{sec}}{n_T} \quad \text{(V)} \tag{17.78}$$

The requirements of the previous equations are summarised in table 17.6 where the maximum on-time is $\hat{t}_{on}$, while the time available for reset is the minimum off-time

$\check{t}_{off}$. The secondary reset voltage V_{sr} requirement and associated dissipated energy W are also included. This table summarises key current transformer requirements as follows

- use a core material which has a low magnetising force, H_s, at saturation
- use a core with a short effective core path length, ℓ_e
- use a high number of turns, N_p and N_s, for a given turns ratio
- operate the transformer with a low secondary voltage, V_{sec}.

Table 17.6. Current transformer requirements showing how magnetic parameter variation affects the electrical characteristics

		core parameters					*circuit parameters*		
		H_s	B_s	B_r	A_e	ℓ_e	N_s	N_p	V_{sec}
Equation (17.75) $t_s = \frac{N_s (B_s - B_r) A_e}{V_{sec}}$	s	*	↑	↓	↑	*	↑	↑	↓
Equation (17.77) $\check{I}_p = \frac{H_s \ell_e}{N_p} \frac{\hat{t}_{on}}{\check{t}_{off}}$	A	↓	*	*	*	↓	*	↑	*
Equation (17.81) $V_{sr} = V_p \frac{\hat{t}_{on}}{\check{t}_{off}}$	V	*	*	*	*	*	*	*	↓
$W = H_s (B_s - B_r) A_e \ell_e \left(\frac{\hat{t}_{on}}{t_s} \right)^2$	J	↓	↓	*	↓	↓	*	*	*
Design requirements		low H_s	—	low B_r	—	low ℓ_e	high turns		low V_{sec}

17.6.5 Current transformer design procedure

Figure 17.18 shows a flowchart design procedure for a current transformer and the design stages are as follows.

Stage 1/stage 2

The current transformer primary and secondary currents, hence turns ratio $n_T = N_s/N_p$, must be specified with the limits on duty cycle times, $\hat{t}_{on}$ and $\check{t}_{off}$. The expected secondary voltage V_{sec} must be specified.

Stage 3

Select a ferrite toroid with an internal diameter, hence window area A_N, sufficient to accommodate the required minimum turns, $n_T + 1$. The copper turns current ratings must be taken into account. The core specifies the effective parameters ℓ_e, A_e, and V_e. The ferrite type specifies B_s, B_r, and H_s.

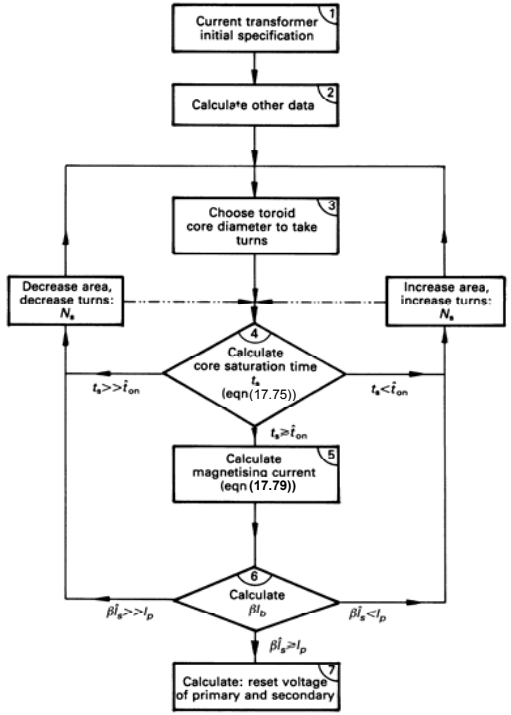

Figure 17.18. *Current transformer design flowchart.*

Stage 4

Calculate the time t_s, before the core saturates from equation (17.75). This time must be greater than the required maximum output current pulse width, $\hat{t}_{on}$.

(i) If $\hat{t}_{on} > t_s$
Either increase the number of turns, using a core with a larger window A_N if necessary.
or increase the core area, A_e, which can be achieved with the same window area, A_N, either with a core of increased thickness or by using two stacked cores.
go to stage 3

(ii) If $t_s >> \hat{t}_{on}$
Either decrease the number of turns which may allow a smaller core size.
or decrease the core cross-sectional area.
go to stage 3

(iii) If $t_s \geqq \hat{t}_{on}$, proceed to stage 5

Stage 5

Calculate the magnetising current at $\hat{t}_{on}$

$$\breve{I}_p = \frac{H_s \ell_e \hat{t}_{on}}{N_p t_s} \quad \text{(A)} \tag{17.79}$$

Stage 6

Calculate the secondary current, taking the magnetising current $\breve{I}_p$ into account

$$\hat{I}_s = \frac{\hat{I}_p - \breve{I}_p}{n_T} \tag{17.80}$$

Is $\beta = \hat{I}_p / I_s$ sufficiently large?
(i) If $\hat{I}_p > \beta \hat{I}_s$
Either decrease the magnetising current by increasing core area.
or increase the turns ratio, n_T.
go to stage 3
(ii) If $\hat{I}_p \ll \beta \hat{I}_s$
Either decrease the turns ratio, n_T.
or decrease the core cross-sectional area.
go to stage 3
(iii) If $\hat{I}_p \lesssim \beta \hat{I}_s$, proceed to stage 7

Stage 7

Calculate the core reset voltage

$$V_{sr} = V_p \frac{\hat{t}_{on}}{\breve{t}_{off}} \quad \text{(V)} \tag{17.81}$$

Calculate the reflected primary on-state voltage

$$e_p = \frac{V_{sr} N_p}{N_s} \tag{17.82}$$

Example 17.7: ***Ferrite current transformer design***

A current transformer primary is used in the collector of a bipolar junction transistor switching circuit and the secondary is used to provide transistor base current as shown in figure 17.20. The maximum collector current is 100 A and the transistor has a gain of 8 at 100 A, in saturation.
The transistor maximum on-time is 46 μs while the minimum off-time is 4 μs. Design a suitable current transformer using the toroid ferrite core, which has low flux leakage and is specified by the data in table 17.5 and appendix 17.7. Assume a core temperature of 25°C.

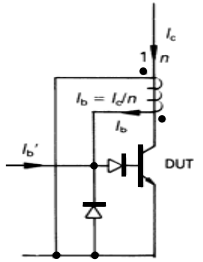

Figure 17.20. *Current transformer for bjt base drive.*

Solution

Based on the flowchart in figure 17.18 and the procedure previously outlined:

Stage 1

The required turns ratio factor is $n_T = N_p/N_s = \beta = 8/1$. In allowing for the magnetising current component, choose $n_T = 15/2$.
The secondary winding voltage is the maximum transistor base to emitter voltage plus the maximum voltage drop across a series diode. Maximum voltage occurs at maximum current.

$$\begin{aligned} V_s &= V_{be_{sat}} + V_D \\ &= 1.2\text{V} + 1.2\text{V} \\ &= 2.4\text{ V} \end{aligned}$$

Stage 2

The current transformer requirements can be summarised as follows

$n_T = N_p/N_s = 15/2$ $\quad\quad$ $\hat{t}_{on} = 46\mu\text{s}$

$V_{sec} = 2.4\text{V}$ $\quad\quad$ $\check{t}_{off} = 4\mu\text{s}$

Stage 3

The ferrite toroid core specified in table 17.5, fulfils the following requirements

$B_s = 0.4$ T at $H_s = 200$ A/m
and $A = 0.398$ cm^2, $\ell_e = 9.71$cm

while the available window area, A_N, is 4.75 cm^2. This window must accommodate two conductor turns of 100 A (plus magnetising current) each and fifteen conductor turns of 12 A each.

Stage 4

The time, t_s, before core saturation is given by equation (17.75), and assuming $B_r = 0$

$$t_s = \frac{15\times0.4\times0.4\text{T}\times10^{-4}}{2.4\text{V}} = 100\ \mu\text{s}$$

Since $t_s > \hat{t}_{on}$, that is 100 μs > 46 μs, proceed to stage 5.

Stage 5

The maximum primary magnetising current, $\hat{I}_p$ is specified by equation (17.79)

$$\hat{I}_p = \frac{46}{100}\times\frac{200\times9.71\times10^{-2}}{2} = 4.47\text{A}$$

Stage 6

The 4.47 A of magnetising current detracts from the primary current available for current transformer action. The maximum available secondary current under worst-case conditions is given by equation (17.80)

$$\hat{I}_s = \frac{100\text{A} - 4.47\text{A}}{15/2} = 12.7\text{A}$$

The maximum allowable collector current is this base current, 12.7 A, multiplied by the transistor gain, 8, which yields 102 A. This is larger than the specified maximum collector current of 100 A, hence the design is correct.

Stage 7

In the on-state, the secondary voltage is 2.4V and the reflected primary voltage is 0.32V.
The maximum secondary voltage, V_{sr}, required to reset the core is given by equation (17.81)

$$V_{sr} = 2.4\text{V}\times\frac{46\mu\text{s}}{4\mu\text{s}} = 27.6\text{V}$$

The reflected primary voltage is 3.7 V.
The reset voltage is usually much larger and is clamped by a base circuit diode in avalanche. Therefore the core reset time will be shorter than 4 μs.
At currents much lower than 100 A, the secondary voltage is decreased, hence the magnetising current is reduced. This reduced magnetising current could consume the full collector current at collector currents of a few amperes. It is therefore necessary to add extra base current to compensate for this deficiency at low currents. The minimum secondary voltage, V_{sec}, specifies the extra requirement according to

$$I_b' = \frac{\check{V}_s}{\hat{V}_s}\times\frac{\hat{I}_p}{n_T} \qquad (17.83)$$

For $\check{V}_s = 1.2$ V, the extra base current requirement is

$$I_b' = \frac{1.2}{2.4}\times\frac{4.47}{7.5} = 300\text{mA}$$

This current can be delivered from an inductive circuit since zero extra current is initially required, and the requirement rises linearly to 300 mA in 46 μs.
A base start pulse of a few microseconds duration is required initially to turn the transistor on, whence collector current is established and current transformer action commences.

♣

17.6 Appendix: Soft ferrite general technical data

Tensile strength	20	N/mm^2
Resistance to compression	100	N/mm^2
Vickers hardness HV_{15}	8000	N/mm^2
Modulus of elasticity	150,000	N/mm^2
Breakage modulus	80-120	N/mm^2
Thermal conductivity	4 - 7× 10^{-3}	J/mm s K (W/mm/K)
Linear expansion coefficient	7-10×10^{-6}	/K
Specific heat	0.75	J/g K
Density	4 - 5	g/cm^3 (4 per cent Si, 7.63 g/cm^3)

Resistivity ρ	$\lambda_s = \frac{\Delta\ell^*}{\ell}$	$\varepsilon_r^{\P} / \rho^{\S}(pu)$				
Ω cm	×10^{-16}	10 kHz	100 kHz	1 MHz	100 MHz	300 MHz
10^5	-18	30/1	15/1	12/1	11/0.97	11/0.95
1	-1.5	140×10^3/1	50×10^3/0.95	30×10^3/0.65	-	-

* Magnetostriction, at saturation, contraction.
¶ Dielectric constant, $\varepsilon_r \rightarrow$ 10-20 at high frequency.
§ Resistivity normalised at low frequency.

17.7 Appendix: Technical data for a ferrite applicable to power applications

Symbol	Unit	Test condition	
μ_i		25°C	2500±20%
$\hat{B}$	T T	25°C 100°C	0.48 0.37
H_s	A/m	B_s = 0.4T, 25°C	200
H	A/m		1600
H_c/B_r	A/m /T	25°C 100°C	12/0.18 9.6/0.11
T_c	°C		>200
ρ	Ω cm		100
η_B^*	mT^{-1} × 10^{-6}	10 kHz	0.9
Density	g/cm^3		4.8
f_c	MHz	25°C	1.8

* - Maximum hysteresis coefficient
10 G (gauss) = 1 mT (milliTesla)
l0 e = 80A/m

17.8 Appendix: Cylindrical inductor design

Figures 17.19a and b show cross-sectional views of single-layer and multi-layer cylindrical inductors. The inductance of a single-layer cylindrical inductor is given by

$$L = \frac{\mu_{eff}(rN)^2}{228.6r + 254\ell} \quad (\mu H) \tag{17.84}$$

while for the multi-layer cylindrical inductor shown in figure 17.19b, inductance is given by

$$L = \frac{\mu_{eff}(rN)^2}{152.4r + 228.6\ell + 254b} \quad (\mu H) \tag{17.85}$$

Figure 17.19c shows a family of curves used to give the effective permeability from the former *l/d* ratio and the core material permeability. These curves are applicable to the single-layer inductor but are a fair approximation of the multi-layer inductor. The winding is assumed to be closely wound over 95 per cent of the core length.

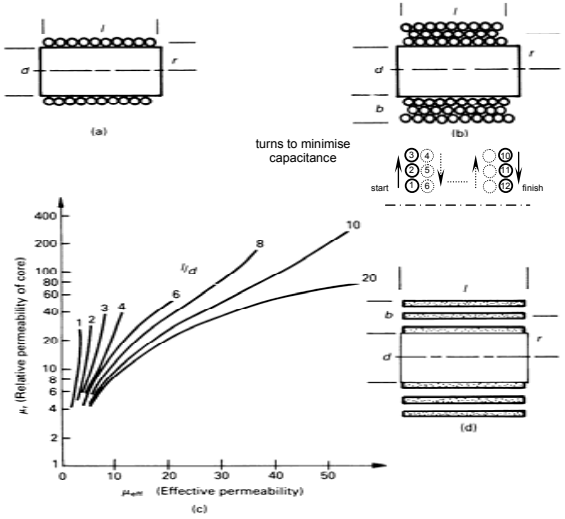

Figure 17.19. *Cylindrical inductors:*
(a) single-layer coil; (b) multi-layer coil; (c) effective permeability for different aspect ratios, lid; and (d) core strip wound air core inductor.

For inductance levels below 100 μH, an air core strip wound inductor as shown in figure 17.19d, has an inductance approximated by

$$L = \frac{r^2 N^2}{225r + 250\ell + 250b + 82.5\dfrac{lb}{r}\left(\dfrac{\ell + 2r}{\ell + 4r}\right)} \quad (\mu H) \qquad (17.86)$$

Inductor design using these equations may require an iterative solution. Always attempt to maximise the winding surface area ($S_A \approx \pi(d + 2b)\ell$) for better cooling.

Example 17.8: ***Wound strip air core inductor***

An air core inductance of 50 μH is made as a wound strip of copper, 40 mm wide and 1.5 mm thick. For cooling purposes, a 0.5 mm spacing is used between each turn with an inner diameter of 60 mm and an outer diameter of 160 mm as physical constraints: Can the required inductance be achieved?

Solution

First calculate the parameters shown in figure 17.18b.

$$r = ¼(d_o + d_i) = ¼ \times (160 + 60) = 55 \text{ mm}$$

$$b = ¼(d_o - d_i) = ¼ \times (160 - 60) = 25 \text{ mm}$$

$$\ell = 40 \text{ mm}$$

$$N = \frac{b}{t_{Cu} + t_{air}} = \frac{50}{1.5 + 0.5} = 25 \text{turns}$$

Substitution of the appropriate parameters into equation (17.86) yields L = 51.6 μH.

♣

Example 17.9: ***Multi-layer air core inductor***

An air core inductor is to have the same dimensions as the inductor in example 17.8. The same conductor area (40 mm × 1.5 mm) but circular in cross-section and number of turns is to be used. Calculate the inductance. If a ferrite cylindrical core 42 mm long and 60 mm in diameter with a relative permeability of 25 is inserted, what will the inductance increase to?

Solution

From example 17.8

r = 55 mm $\qquad$ ℓ = 40 mm

b = 50mm $\qquad$ N = 25

Substitution of these parameter values into equation (17.85) yields 62.5 μH.

From figure 17. 18c, ℓ/d = 40/60 = 0.66, whence $\mu_{eff} \approx 3$. That is, with a cylindrical core inserted, a three fold increase in inductance would be expected (188 μH).

The use of end-caps and an outer magnetic sleeve would increase inductance, but importantly also help to contain the stray magnetic field.

♣

17.9 Appendix: Copper wire design data

Nominal wire diameter d	Outer diameter enamelled grade 2	Approximate dc resistance at 20°C	Bare copper weight	Fusing current
mm	mm	Ω/m	gm/m	A
0.1	0.129	2.195	0.070	2.5
0.2	0.245	0.5488	0.279	7
0.376	0.462	0.136	1.117	18
0.5	0.569	8.781×10^{-2}	1.746	27.5
0.6	0.674	6.098×10^{-2}	2.50	36
0.8	0.885	3.430×10^{-2}	4.469	57
0.95	1.041	2.432×10^{-2}	6.301	79
1	1.093	2.195×10^{-2}	6.982	82
1.5	1.608	9.67×10^{-3}	15.71	145
2	2.120	5.44×10^{-3}	27.93	225
2.5	2.631	3.48×10^{-3}	43.64	310
3	3.142	2.42×10^{-3}	62.84	>
4	4.160	1.36×10^{-3}	111.7	>
4.5	4.668	1.08×10^{-3}	141.4	>
5.0	5.177	8.70×10^{-4}	174.6	>

17.10 Appendix: Minimisation of stray inductance

In many circuit layouts, it is essential to minimise stray and residual inductance. With high *di*/*dt* currents during switching, large voltages occur ($v = L\ di/dt$) which may impress excessive stresses on devices and components. Stray inductance within a package reduces its usable voltage rating. Stray inductance in the drain circuit of the MOSFET, within the package as shown in figure 4.17, reduces the usable voltage rail while source inductance increases the transient gate voltage. In the case of capacitors, residual inductance reduces the effectiveness of turn-off snubbers and can result in an unintentional resonant circuit.

Inductance of a straight wire of length ℓ and radius r is

$$L = \frac{\mu_o \ell}{2\pi}\left(\ell n\frac{2\ell}{r} - \tfrac{3}{4}\right) \quad \text{(H)} \qquad (17.87)$$

which as a rule of thumb is about 1μH/m.

17.10.1 Reduction in wiring residual inductance

Wiring inductance can be decreased by cancelling magnetic fields in a number of ways

- coaxial cable
- parallel plates
- parallel wiring conductors.

In each case, the go and return paths are made parallel and physically close. Figure 17.21 shows the per unit length inductance for each wiring method.

coaxial cable

Minimum inductance results with coaxial cable, which is available for power application. The per unit inductance and capacitance are given by

$$L = \frac{\mu_o \mu_r}{2\pi}\ell n\frac{r_o}{r_i} \quad \text{(H/m)}$$
$$C = 2\pi\varepsilon_o\varepsilon_r / \ell n\frac{r_o}{r_i} \quad \text{(F/m)} \qquad (17.88)$$

where r_i is the inner radius and r_o the outer radius.

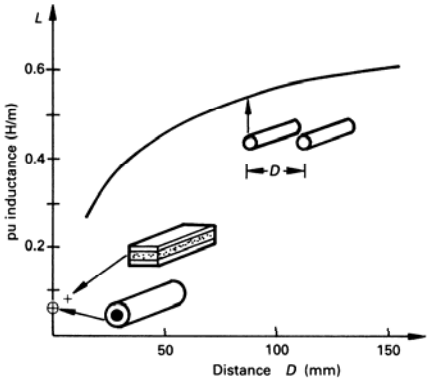

Figure 17.21. *Inductance of go and return wiring conductors.*

parallel plates

Very low inductance can be achieved by using parallel conducting copper plates separated by a thin insulation layer. The inductance per unit length, neglecting skin effects, is approximated by

$$L = \mu_o \frac{d}{w} \quad \text{(H/m)} \qquad (17.89)$$

where d is the separation of the plates and
w is the plate width.

The parallel plate capacitance is

$$C = \varepsilon_o\varepsilon_r\, w/d \quad \text{(F/m)} \qquad (17.90)$$

A complete analysis of the laminated parallel bus bar configuration is presented in appendix 17.11

parallel wiring conductors

For parallel wiring cylindrical conductors of radius r and separation D, in air,

$$C = \frac{2\pi\varepsilon_o}{\ell n\left(\frac{D}{r}\right)} \quad \text{(F/m)}$$
$$L = \frac{\mu_o}{\pi}\ell n\left(\frac{D}{r}\right) \quad \text{(H/m)} \qquad (17.91)$$

When the separation is small over a long distance, ℓ, that is $D/\ell \ll 1$, the capacitance, inductance, and mutual coupling inductance are

$$C = \frac{\pi\varepsilon_o}{\cosh^{-1}\left(\frac{D}{2r}\right)} \quad \text{(F/m)}$$
$$L = \frac{\mu_o \ell}{\pi}\left\{\ell n\left(\frac{D}{r}\right) - \frac{D}{\ell} + \tfrac{1}{4}\right\} \quad \text{(H)} \qquad (17.92)$$
$$M = \frac{\mu_o \ell}{2\pi}\left\{\ell n\left(\frac{D}{r}\right) - \frac{D}{\ell} - 1\right\} \quad \text{(H)}$$

parallel wiring conductors over a conducting ground plane

The self inductance and mutual inductance between two conductors height h over a ground plane carrying the return current are given by

$$L = \frac{\mu_o}{2\pi}\ell n\frac{2h}{r} \quad \text{(H/m)}$$
$$M = \frac{\mu_o}{4\pi}\ell n\left(1 + \left(\frac{h}{r}\right)^2\right) \quad \text{(H/m)} \qquad (17.93)$$

Figure 17.21 shows that go and return power cable residual inductance decreases as separation decreases. Physical and mechanical constraints may dictate which wiring technique is most viable. All other wiring should cross perpendicularly, in order to minimise coupling effects.

Inductance of other conductor profiles

The self-inductance of a rectangular conductor, not associated with a return path in close proximity is

$$L = \frac{\mu_o}{2\pi}\left[\ell n\left(\frac{2\ell}{w+t}\right) + \tfrac{1}{2} + \frac{2}{9}\frac{w+t}{\ell}\right] \quad \text{(H/m)} \qquad (17.94)$$

When the bus bar and its return path are side-by-side in the same plane

$$L = \frac{\mu_o}{2\pi}\left[\ell n\left(\frac{D}{w+t}\right) + \frac{3}{2}\right] \quad \text{(H/m)} \qquad (17.95)$$

or long cylindrical wire and its return path are side-by-side in the same plane

$$L = \frac{\mu_{wire}}{8\pi} + \frac{\mu}{2\pi}\ell n\frac{D}{r} \quad \text{(H/m)} \qquad (17.96)$$

where w is the width of the conductors
t is the thickness of the conductors
D is the distance between the midpoints of the conductors
ℓ is the conductor length.

The first component in equation (17.96) is the internal self-inductance component, which for copper and aluminium, $\mu_{wire} = \mu_o$, gives 50nH per metre.

17.10.2 Reduction in component residual inductance

17.10.2i - Capacitors

The inductance of a cylindrical capacitor winding, employing extended foils and scooping connections is given by

$$L = \frac{\mu_o}{2\pi}\left[\ell n\frac{2b}{r} - \tfrac{3}{4}\right] \quad \text{(H)} \qquad (17.97)$$

where b is the length of the cylinder winding and $2r$ is its diameter. This equation shows that inductance is decreased by decreasing the length and by increasing the diameter.

17.10.2ii - Capacitors - parallel connected

Capacitors are extensively parallel connected, by manufacturers before potting, or by the user after potting, in order to increase capacitance. The low inductance feature of an extended foil, scoop connected capacitor can be obliterated by poor lead connection. Consider the parallel-connected capacitors shown in figure 17.22a, which shows the

relative residual wiring inductance for three connections. Minimum inductance results when using a thin, double-sided copper printed circuit board arrangement, such that connections alternated between the top and bottom copper layers (go and return conductors). Cutouts in the pcb, for the capacitors to fit into, only marginally decrease the inductance.

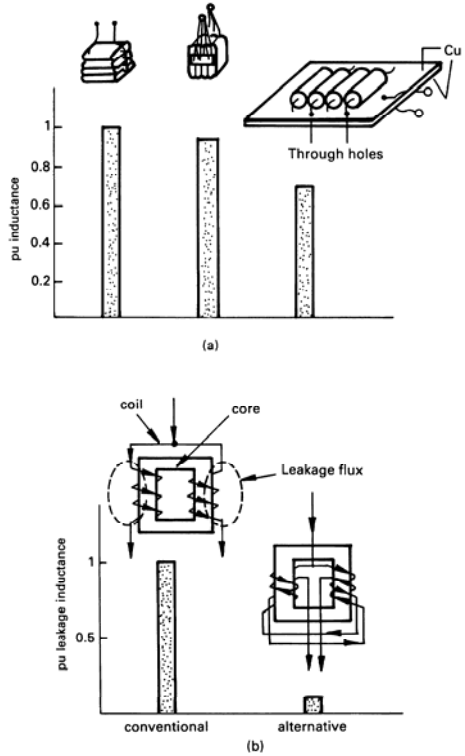

Figure 17.22. *(a) Parallel connected capacitors, inductance and (b) leakage inductance of a current balancing transformer.*

***17.10.2iii* -** Transformers

A current balancing transformer may be used to equalise the principal currents of two parallel-connected power devices, as shown in figure 10.8. Conventionally each coil is wound on separate legs of the core, resulting in a large leakage inductance. This large leakage inductance can result in high voltage transients, which are to be avoided.
Leakage can be significantly decreased if two coils are bifilar wound on each limb and connected as shown in figure 17.22b. The same leakage flux cancelling technique can be used on the centre-tapped, push-pull transformer for the switch mode power supply shown in figure 15.8. Because of the close proximity of bifilar wound conductors, high interwinding capacitance and high dielectric fields may be experienced.

17.11 Appendix: *Laminated bus bar design*

As shown in figure 17.21, the use of a parallel laminated bus bar arrangement shown in figure 17.23a for go and return paths, results in a low inductance loop. If the gap between the bus bars is laminated with a dielectric material, distributed capacitance properties are gained.
A laminated bus bar arrangement offers the following features:

- high packing density
- better conductor cooling because of flat surface area
- low voltage drop
- high voltage and current capability
- reliable and eliminates wiring errors
- space saving
- increased capacitance for better noise suppression
- low inductance because thin parallel conductors allow flux cancellation

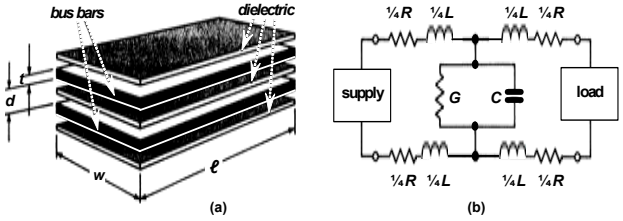

Figure 17.23. *Laminated bus bar:*
(a) Parallel planar construction and (b) equivalent circuit distributed components.

The physical bus bar dimensions are related to the electrical parameters and characteristics. The two level bus bar comprises two parallel conducting plates of aluminium, brass or copper with resistivity σ, separated by a dielectric, with dielectric constant ε_r, and permeability μ_o, giving a conductance G, capacitance C, and resistance R which are uniformly distributed along the bus, as shown in figure 17.23b.

Capacitance, C
The capacitance C is given by

$$C = \varepsilon_o \varepsilon_r \frac{w}{d} \qquad \text{(F/m)} \tag{17.98}$$

where w is the width of the conductors
d is the distance between the bars, which is the dielectric thickness.
An increase in capacitance decreases the characteristic impedance, $Z_o = \sqrt{L/C}$. A lower impedance gives greater effective signal suppression and noise elimination. This is achieved with

- a smaller bar separation, d,
- a higher permittivity dielectric material, ε_r,
- wider conductors, w.

Shunt conductance, G
The shunt conductance G depends on the quality of the dielectric, specifically its conductivity at the operating frequency.

$$G = \frac{1}{\sigma}\frac{w}{d} \qquad \text{(℧/m)} \tag{17.99}$$

Skin effect
Both the resistance and inductance are affected by the ac skin effect, which is frequency dependant. This was briefly treated in section 17.3.4ii, and specifically equation (17.36). The skin effect is when at high frequencies the current tends to flow on the surface of the conductor. The skin depth δ, from equation (17.36)

$$\delta(f) = \sqrt{\rho / \mu_o \pi f} \tag{17.100}$$

where ρ is the resistivity of the conductor at frequency f.
The skin depth for copper and brass are

$$\delta_{Cu} = \frac{0.066}{\sqrt{f}} \quad \text{(m)} \qquad \delta_{Brass} = \frac{0.126}{\sqrt{f}} \quad \text{(m)} \tag{17.101}$$

As the frequency increases L decreases and R increases.

Inductance, L

There two inductive components,

- L_{int} - inside the conductor due to internal flux linkages,
- L_{ext} - external inductance between the two conductors due to the orientation of the two conductor carrying current.

In power applications and at the associated frequencies, the external inductance is more dominant.

$$L_{ext} = \mu_o \frac{d}{w} \quad \text{(H/m)} \tag{17.102}$$

At high frequency (taking the skin effect into account) the effective inductance is

$$L_e = \mu_o \frac{d+\delta}{w} \quad \text{(H/m)} \tag{17.103}$$

Thus to decreased inductance

- decrease the dielectric thickness, d
- increase the conductor width, w
- decrease the skin depth δ by using a conductor of lower resistivity.

Resistance, R

The dc resistance R_{dc} of the two conductors is

$$R_{dc}(20°\text{C}) = 2\rho \frac{1}{wt} \quad (\Omega/\text{m}) \tag{17.104}$$

where t is the thickness of the conductors

The resistivity of copper and brass at 20°C are 1.7×10^{-8} and 7.0×10^{-8} Ωm, respectively.

The temperature effects on resistance for copper are accounted for by

$$R_{T_o} = R_{20°C}\left(1 + 0.0043\times(T_o - 20°C)\right) \quad (\Omega) \tag{17.105}$$

At high frequency, taking the skin effect into account, assuming that the conductor thickness is at least twice the skin depth,

$$R_{ac} = 2\rho \frac{2}{\delta w} \quad (\Omega/\text{m}) \tag{17.106}$$

Characteristic impedance, Z

The characteristic impedance Z of the go-and return bus bar arrangement is given by

$$Z = \sqrt{\frac{R + j\omega L}{G + j\omega C}} \quad (\Omega) \tag{17.107}$$

when the conductor resistance R and insulation conductance G are negligible

$$Z = \sqrt{\frac{L}{C}} \quad (\Omega) \tag{17.108}$$

This equation illustrates that increasing the capacitance and decreasing the inductance reduces bus bar noise problems. Common to decreased inductance and increased

capacitance are

- decrease the dielectric thickness d and
- increase the bus bar width w

That is, characteristic impedance Z is proportional to d/w.

Figure 17.24 compares the electrical parameters obtained for one metre of twist pair plastic coated 1mm diameter solid copper wire and one metre of laminated bus bar. The copper cross section area is the same in each case, giving a dc resistance of 44mΩ per metre. The most significant electrical factor is the reduction in inductance when a bus bar arrangement is used. Better electrical parameters are gained for a significant cost increase.

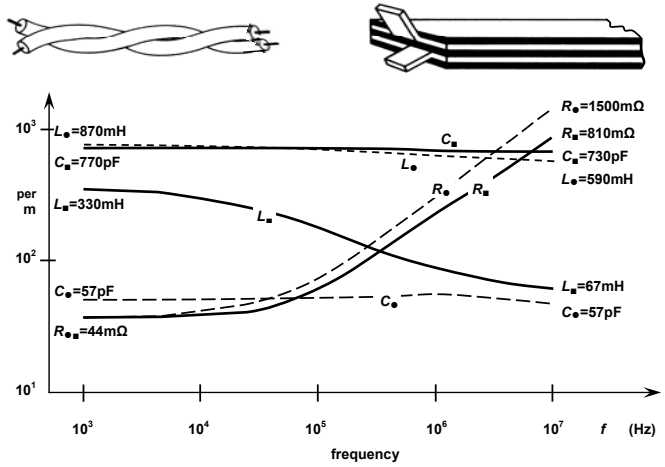

Figure 17.24. *Comparison between electrical parameters for a twisted pair and a laminated bus bar, each with the same copper cross sectional area, that is, the same dc resistance.*

Reading list

McLyman, W. T., *Transformer and Inductor Design Handbook*,
Marcel Dekker Inc., 1978.

Snelling, E. C., *Soft Ferrites*,
CRC Press, Cleveland, Ohio, 1969.

Manufacturers Data Handbooks and Catalogues

Siemens	Thomson CSF	Philips
SEI	Telmag	Neosid
Magnetics Inc	Krystinel Corp	Stackpole
Ferroxcube Inc	Arnold Eng. Co.	Micrometals Co.
Pyroferric Inc	Fuji	

Problems

17.1. Rework example 17.7, taking $B_r = 0.18$ T into account.

17.2. Rework example 17.7, when the core temperature is 100°C.

17.3. Rework example 17.3 when

$V_e = 7.3 \times 10^{-6}$ m^3 $\quad A_e = 66$ mm^2

$\ell_e = 110$ mm $\quad c = 0.75$ nH

What are the effects of decreasing the core volume for a given L and I?
[10A: 274 J/m^3, 0.53 mm, 1200 A/m, 13 turns; 20A: 2360 A/m, $\mu_e = 185$]

17.4. Show that the maximum flux density for a square-wave-excited transformer is given by

$$\hat{B} = \frac{V}{4NAf}$$

17.5. A 2:1 step-down transformer with an effective area of 10 cm^2 is driven from a 240 V, 1 kHz square-wave source. The transformer has 240 primary turns and magnetising inductance of 10 mH.

i. Calculate the maximum flux density.

ii. Calculate the peak primary current when the secondary is loaded with a 5 Ω resistor. Sketch the primary and secondary current waveforms.
[0.25 T, 30 A]